

**Pseudogap and spectral function from superconducting fluctuations to the bosonic limit**A. Perali,<sup>1,2</sup> P. Pieri,<sup>1</sup> G. C. Strinati,<sup>1</sup> and C. Castellani<sup>2</sup><sup>1</sup>Dipartimento di Matematica e Fisica, Sezione INFN, Università di Camerino, Via Madonna delle Carceri, I-62032 Camerino, Italy<sup>2</sup>Dipartimento di Fisica, Sezione INFN, Università di Roma "La Sapienza," P.le A. Moro, 2, I-00185 Roma, Italy

(Received 6 February 2002; published 3 July 2002)

The crossover from weak to strong coupling for a three-dimensional continuum model of fermions interacting via an attractive contact potential is studied above the superconducting critical temperature  $T_c$ . The pair-fluctuation propagator, the one-loop self-energy, and the spectral function are investigated in a systematic way from the superconducting fluctuation regime (weak coupling) to the bosonic regime (strong coupling). Analytic and numerical results are reported. In the strong-coupling regime, where the pair fluctuation propagator has bosonic character, two quite different peaks appear in the spectral function at a given wave vector, a broad one at negative frequencies and a narrow one at positive frequencies. The broad peak is asymmetric about its maximum, with its spectral weight decreasing by increasing coupling and temperature. In this regime, two crossover temperatures  $T_1^*$  (at which the two peaks in the spectral function merge in one peak) and  $T_0^*$  (at which the maximum of the lower peak crosses zero frequency) can be identified, with  $T_c \ll T_0^* < T_1^*$ . By decreasing coupling, the two-peak structure evolves smoothly. In the weak-coupling regime, where the fluctuation propagator has diffusive Ginzburg-Landau character, the overall line shape of the spectral function is more symmetric and the two crossover temperatures approach  $T_c$ . The analysis of the spectral function identifies specific features which allow one to distinguish by ARPES whether a system is in the weak- or strong-coupling regime. Connection of the results of our analysis with the phenomenology of cuprate superconductors is also attempted.

DOI: 10.1103/PhysRevB.66.024510

PACS number(s): 74.20.-z, 74.25.Jb

**I. INTRODUCTION**

High- $T_c$  cuprate superconductors are characterized by doping- and temperature-dependent anomalous properties in the metallic and superconducting phases. At low doping, the cuprates display a *pseudogap* in the single-particle excitation spectra and in the spin susceptibility, above the superconducting critical temperature  $T_c$  and below a crossover temperature  $T^*$ . The temperature  $T^*$  decreases with increasing doping and merges eventually to  $T_c$  close to optimum doping.<sup>1</sup> The pseudogap phase of underdoped cuprates is best characterized by angle resolved photoemission spectroscopy (ARPES) (Refs. 2–4) and by tunneling experiments.<sup>5,6</sup> The pseudogap opening below  $T^*$  corresponds to a suppression of the low-frequency differential conductance (which is connected to the density of states) measured by tunneling, and to a leading-edge shift of the spectral intensity (which is connected to the spectral function via the Fermi distribution and a dipole matrix element) measured by ARPES. As clearly shown by ARPES, the pseudogap is tied to the Fermi surface and its two-dimensional wave-vector dependence resembles a  $d_{x^2-y^2}$  harmonic. Both ARPES and tunneling experiments suggest that the pseudogap evolves smoothly into the superconducting gap as the temperature is lowered from  $T^*$  to  $T_c$ .

The  $d$ -wave-like wave-vector dependence of the pseudogap, its continuous evolution into the superconducting gap below  $T_c$ , and its tying to the Fermi surface suggest that the pseudogap phase could be a *precursor* of the superconducting phase (at least in Bi-based compounds for which a detailed ARPES analysis of the pseudogap is available). According to this interpretation, the crossover temperature  $T^*$  acquires the meaning of the temperature at which fluctuating

pairs start forming without coherence, the latter being not yet established owing to large fluctuations of the superconducting order parameter. Upon lowering the temperature, the coherence between pairs is established and superconductivity appears. The occurrence of large pair fluctuations in cuprates is related to the quasibidimensionality, as well as to the short coherence length  $\xi_0$  of the Cooper pairs (typically,  $\xi_0 \sim 10 - 20 \text{ \AA}$ ).

Within this scheme, the phase diagram of cuprates is interpreted in terms of a *crossover* from Bose-Einstein (BE) condensation of preformed pairs to BCS superconductivity, as the doping is varied.<sup>7–19</sup> Heavily underdoped cuprates are accordingly considered as superconductors in a strong-coupling (BE) regime with  $T^* \gg T_c$ ; optimally doped and overdoped cuprates are instead more conventional superconductors in an intermediate- or weak-coupling (BCS) regime with  $T^* \approx T_c$ . The evolution from strong- to weak-coupling superconductivity as the doping is increased is further supported by low-temperature ARPES and tunneling measurements in Bi-based compounds of the maximum superconducting gap  $\Delta_0$ , whereby  $\Delta_0$  decreases as the doping is increased, with  $\Delta_0 \approx 60 - 70 \text{ meV}$  in underdoped cuprates and  $\Delta_0 \approx 20 - 30 \text{ meV}$  in optimally and overdoped cuprates.<sup>5,6</sup> Moreover, in underdoped Bi-based cuprates  $\Delta_0$  is larger than the bandwidth along the  $M - Y(X)$  directions, suggesting that at least near the  $M$  points states with bosonic character can be formed. Recent ARPES measurements on  $\text{La}_{2-x}\text{Sr}_x\text{CuO}_4$  also indicate a similar doping dependence of the gap.<sup>20</sup>

Recent high-resolution ARPES experiments in Bi2212 further suggest that a crossover from weak to strong coupling can even be found *along* the Fermi surface (FS) at fixed doping.<sup>21</sup> Fermionic states near the nodal ( $N$ ) points of the

FS (namely, the points where the  $d$ -wave gap vanishes) appear to be weakly coupled, while states near the  $M$  points are strongly coupled and could display bosonic character. In agreement with the expectation that increasing the coupling should cause an increase of the width of the spectral peaks, explicit support to the wave-vector induced crossover along the FS is obtained, for instance, from Fig. 2 of Ref. 21. The ARPES spectral intensities for an optimally doped Bi2212 sample reported in that figure show, in fact, that the width of the quasiparticle peak in the normal phase increases along the FS, as one moves from the  $N$  toward the  $M$  point. In particular, near the  $M$  points the frequency distribution of the spectral intensity is broad and flat without any observable peak, while a broad peak feature is present in the wave-vector distribution. In addition, in Bi2212 at optimum doping the band dispersion near the  $M$  points along the  $M-Y(X)$  direction is rather narrow ( $\sim 50$  meV), while the band dispersion along the  $\Gamma-Y(X)$  directions is considerably larger ( $\sim 400$  meV). For all cuprates for which ARPES measurements are available, the Fermi velocity  $v_F$  is also anisotropic along the Fermi surface, with  $v_F(N)/v_F(M) \approx 3$ .<sup>22</sup> As a consequence, fermionic states near the  $M$  points are locally associated with a small Fermi velocity and strong coupling (hot fermions); while fermionic states near the  $N$  points are locally associated with a large Fermi velocity and weak coupling (cold fermions). To account explicitly for the different properties about the  $M$  and  $N$  points, a two-gap model has been recently proposed.<sup>23</sup>

In the present paper, we investigate the evolution of the spectral function from the weak- to strong-coupling regimes in a systematic way, to compare with the evolution of the spectral function in cuprates by varying doping and wave vector. More specifically, we aim to account for the character of the fermionic states near the  $M$  points (where bosonic states can be formed upon reducing the doping due to the *hot* character of these states) and to follow the wave-vector induced crossover along the Fermi surface. The local character of the fermionic states in wave-vector space further enables us to use a simple isotropic attraction between electrons, which gives rise in the superconducting state to a gap with  $s$ -wave symmetry.

Two different (albeit related) kinds of approaches for the pseudogap state can be identified within the pairing scenario. On the one hand, owing to the short coherence length and the large value of the superconducting gap about the  $M$  points,<sup>7-16,18,19</sup> the superconducting phase of underdoped cuprates is interpreted as intermediate between a BCS state with extended pairs and a Bose-Einstein condensate with preformed (local) pairs. Within this view, due to strong- or intermediate-coupling effects, pairing correlations survive well above  $T_c$  and determine a pseudogap opening when coupled to the fermions. On the other hand, the second approach emphasizes the relevance of phase fluctuations of the superconducting order parameter, owing to the low value of the plasma frequency and the quasibidimensionality of the cuprates.<sup>24-27</sup> Within this view, the amplitude of the local order parameter is established at  $T^*$ , even though phase coherence and hence long-range superconductivity occurs at the lower temperature  $T_c$ .

The approach we follow in this paper belongs to the first group of the pairing scenario. Specifically, we investigate the role played by pair fluctuations in the pseudogap opening, following the BCS to Bose-Einstein crossover from weak to strong coupling. To this end, we introduce a simplified microscopic model representing a three-dimensional (3D) continuum of fermions mutually interacting via an attractive contact potential, which can be parametrized in terms of the scattering length. This 3D model allows us to considerably simplify the numerical calculations as well to obtain analytic results (at least in some limits), yet preserving the qualitative features obtained for more realistic models, such as the two-dimensional negative-U Hubbard model.<sup>28-31</sup>

We examine initially the two-particle propagator in the particle-particle channel, and evaluate the pair-fluctuation propagator  $\Gamma(\mathbf{k}, \omega)$  as a function of wave vector  $\mathbf{k}$  and frequency  $\omega$ . We further analyze the *single-particle* propagator, and evaluate the self-energy  $\Sigma(\mathbf{k}, \omega)$  and the spectral function  $A(\mathbf{k}, \omega)$  within the non-self-consistent  $t$ -matrix approximation. In the strong- and weak-coupling regimes, we discuss *analytic* forms for the self-energy, and comment on the main differences in the line shape of  $A(\mathbf{k}, \omega)$  between the two regimes. The spectral weight of the incoherent peak that appears in  $A(\mathbf{k}, \omega)$  and the temperature dependence of the chemical potential are also discussed. In the intermediate (crossover) region (where analytic calculations are not feasible) only numerical results are presented. Our findings of different characteristic features occurring for  $A(\mathbf{k}, \omega)$  in different coupling regimes are then organized in a systematic way, and a criterion to distinguish by ARPES experiments whether an interacting fermion system is in the strong-, intermediate-, or weak-coupling regime is discussed. In the strong-coupling regime, we find it is appropriate to introduce two different crossover temperatures ( $T_1^*$  and  $T_0^*$ ) to describe the peculiar evolution of the spectral function for increasing temperature. We also show how these two temperatures merge to a single crossover temperature ( $T^*$ ) as the coupling is decreased. A detailed comparison of ARPES experiments with our analysis of the spectral function in different coupling regimes is eventually attempted. Although it might at first appear that our model could not be directly applied for comparison with ARPES experiments in cuprates, this comparison is attempted by invoking the wave-vector-induced crossover mentioned above. Even though some parts of our analysis and results have been already presented (albeit for different models and/or with different methods) in previous work,<sup>28,16,17,19</sup> our approach should be regarded as more systematic and complete than others.

The plan of the paper is as follows. In Sec. II we introduce the microscopic model and discuss the relevant equations for the spectral function and related quantities. In Secs. III and IV we report the results for two- and single-particle properties, respectively, discussing the evolution of the pair-fluctuation propagator and of the spectral function from the superconducting fluctuations regime (weak coupling) to the bosonic limit (strong coupling). In Sec. V we present a detailed comparison of our results with ARPES experiments. Section VI gives our conclusions.

## II. RELEVANT EQUATIONS FOR THE SPECTRAL FUNCTION AND RELATED QUANTITIES

In this section, we set up the relevant equations to follow the evolution of the single-particle spectral function and the two-particle fluctuation propagator from weak to strong coupling. To this end, we consider a system of fermions embedded in a three-dimensional continuum and mutually interacting via an effective short-range attractive potential  $v_0 \delta(\mathbf{r} - \mathbf{r}')$  of strength  $v_0$ , where  $v_0$  is a negative constant. For the 3D continuum model we are allowed to take the limit of a strictly short-range interaction, thus relating to the fermionic scattering length  $a_F$  by a suitable regularization procedure. Knowledge of the detailed form of the fermionic interaction is, in fact, not required for studying the main features of the evolution from weak to strong coupling. The many-body diagrammatic structure for the single- and two-particle Green's functions gets in this way considerably simplified, while preserving the physical effects of pseudogap opening.<sup>32</sup> (For a detailed discussion of this model, see Ref. 33.)

For the attractive fermionic interaction of interest, the scattering length  $a_F$  changes from being negative (when the two-body problem fails to support a bound state) to being positive (when the bound state is eventually supported by increasing the interaction strength), and diverges when the coupling strength suffices for the bound state to appear. The dimensionless parameter  $k_F a_F$  (where  $k_F$  is the Fermi wave vector) thus locates the side of the crossover one is examining and how close to the crossover region one is. Specifically,  $k_F a_F$  is small and negative in the weak-coupling regime, diverges in the intermediate (crossover) regime, and eventually becomes small and positive in the strong-coupling regime. For this reason, driving the crossover by varying  $k_F$  while keeping  $a_F$  fixed requires one to change discontinuously the sign of  $a_F$  at the value  $(k_F a_F)^{-1} = 0$ .

The diagrammatic scheme we consider is based on the non-self-consistent  $t$ -matrix approximation, constructed with “bare” single-particle Green's functions [with the inclusion, however, of the dressed chemical potential and of an additional constant energy shift (to be discussed below) which is relevant to the symmetry of the spectral function]. This choice embodies the physics of the pseudogap state, because in the weak-coupling regime it describes the Ginzburg-Landau superconducting fluctuations above  $T_c$ ,<sup>34</sup> while in the strong-coupling regime it describes the formation of non-interacting bosons (fermionic bound states).<sup>35</sup>

The set of relevant equations for the two-particle Green's function in the particle-particle channel (i.e., the pair-fluctuation propagator), the single-particle Green's function, and the self-energy is the following:

$$\begin{aligned} \Sigma(\mathbf{k}, \omega_n) = & -T \sum_{\nu} \int \frac{d^3 q}{(2\pi)^3} \Gamma^{(0)}(\mathbf{q}, \Omega_{\nu}) \\ & \times G^{(0)}(\mathbf{q} - \mathbf{k}, \Omega_{\nu} - \omega_n), \end{aligned} \quad (1)$$

$$\begin{aligned} \Gamma^{(0)-1}(\mathbf{q}, \Omega_{\nu}) = & -\frac{m}{4\pi a_F} - \int \frac{d^3 k}{(2\pi)^3} \\ & \times \left[ T \sum_n G^{(0)}(\mathbf{k}, \omega_n) \right. \\ & \left. \times G^{(0)}(\mathbf{q} - \mathbf{k}, \Omega_{\nu} - \omega_n) - \frac{m}{k^2} \right], \end{aligned} \quad (2)$$

$$G^{-1}(\mathbf{k}, \omega_n) = G^{(0)-1}(\mathbf{k}, \omega_n) - [\Sigma(\mathbf{k}, \omega_n) - \Sigma_0], \quad (3)$$

$$n = 2T \sum_n e^{i0^+ \omega_n} \int \frac{d^3 k}{(2\pi)^3} G(\mathbf{k}, \omega_n). \quad (4)$$

Here,  $G^{(0)}(\mathbf{k}, \omega_n)$  is the “bare” fermion propagator given by  $G^{(0)-1}(\mathbf{k}, \omega_n) = i\omega_n - \xi(\mathbf{k})$  [ $\xi(\mathbf{k}) = \mathbf{k}^2/(2m) - \mu'$  being the free-particle dispersion measured with respect to the renormalized chemical potential  $\mu' = \mu - \Sigma_0$ , where  $\mu$  is the physical chemical potential and  $\Sigma_0$  the constant self-energy shift mentioned above],  $m$  is the free-fermion mass, and  $\omega_n = \pi T(2n+1)$  ( $n$  integer) and  $\Omega_{\nu} = 2\pi T\nu$  ( $\nu$  integer) are, respectively, fermionic and bosonic Matsubara frequencies at temperature  $T$ . The chemical potential is eliminated in favor of the density  $n$  via Eq. (4). The constant self-energy shift  $\Sigma_0$  is given by  $\text{Re} \Sigma(k=k_{\mu'}, \omega=0, T \sim T^*)$  where  $k_{\mu'} = \sqrt{2m\mu'}$ . It turns out that this shift is non-negligible only in the weak- to intermediate-coupling regime, where it is almost temperature independent from  $T$  to  $T^*$ . (In this coupling regime,  $T^* = T_0^* = T_1^*$  is the temperature at which the pseudogap disappears.) In practice, we will take  $\Sigma_0 = \text{Re} \Sigma(k=k_{\mu'}, \omega=0, T=T_c)$  in the weak- to intermediate-coupling regime, while we shall neglect  $\Sigma_0$  altogether in the intermediate- to strong-coupling regime. Inclusion of this self-energy shift amounts to a partial self-consistency dressing of the single-particle Green's functions  $G^{(0)}$ , and corresponds to a complete description of the high-temperature region.

After analytic continuation to the real frequency axis,<sup>36</sup> the imaginary part of the retarded self-energy can be written at this order of approximation in the form

$$\begin{aligned} \text{Im} \Sigma(\mathbf{k}, \omega) = & - \int \frac{d^3 q}{(2\pi)^3} \{ b[\omega + \xi(\mathbf{q} - \mathbf{k})] + f[\xi(\mathbf{q} - \mathbf{k})] \} \\ & \times \text{Im} \Gamma^{(0)}[\mathbf{q}, \omega + \xi(\mathbf{q} - \mathbf{k})], \end{aligned} \quad (5)$$

where  $f(x) = 1/(e^{\beta x} + 1)$  is the Fermi distribution and  $b(x) = 1/(e^{\beta x} - 1)$  is the Bose distribution, with  $\beta = 1/T$ . Hereafter, analytic continuations are meant to produce retarded ( $R$ ) functions. Once the imaginary part of the self-energy is evaluated as above, its real part  $\text{Re} \Sigma(\mathbf{k}, \omega)$  is obtained via a Kramers-Kronig transform. The real-frequency formulation (5) allows for high accuracy of the numerical calculations, and avoids the problems of dealing numerically with analytic continuation from the imaginary frequency axis.

The spectral function  $A(\mathbf{k}, \omega)$  for the single-particle fermionic excitations of interest is obtained from the imaginary part of the retarded Green's function  $G^R(\mathbf{k}, \omega)$  via the relation

$$A(\mathbf{k}, \omega) = -\frac{1}{\pi} \text{Im} G^R(\mathbf{k}, \omega). \quad (6)$$

In terms of the real and imaginary parts of the self-energy, the spectral function  $A(\mathbf{k}, \omega)$  has the form

$$A(\mathbf{k}, \omega) = \frac{-\text{Im} \Sigma(\mathbf{k}, \omega) / \pi}{[\omega - \xi(\mathbf{k}) - \text{Re} \Sigma(\mathbf{k}, \omega) + \Sigma_0]^2 + [\text{Im} \Sigma(\mathbf{k}, \omega)]^2}. \quad (7)$$

The set of equations (1)–(5), together with the definition of the spectral function (7) and the prescription for analytic continuation to real frequencies, allows us to study in a *systematic way* with limited computational effort two- and single-particle properties over a wide range of parameters (namely, coupling, density, and temperature), following the crossover from weak to strong coupling.

A few additional comments are in order at this point about the choice (1) of the self-energy. In the weak-coupling regime and at high enough temperature, the expression (1) represents the leading term of a low-density expansion for a Fermi system even when the interaction is attractive.<sup>33</sup> Upon approaching  $T_c$ , the expression (1) can alternatively be interpreted as representing the coupling of a bare fermion with pairing fluctuations. In the strong-coupling regime, the expression (1) represents instead a “free” boson coupled to a bare fermion, and is known to produce a shadow-band structure in the spectral function at negative frequencies.

Finally, we recall that inclusion of full self-consistency in the single-particle Green's functions entering Eq. (1) can be safely dismissed [at least in the weak- and strong-coupling regimes, where the use of expression (1) can be justified to start with], as discussed in Ref. 33. In contrast to the non-self-consistent  $t$ -matrix approximation used in Eqs. (2)–(4), the self-consistent  $t$  matrix uses full self-consistent Green's functions but does not include vertex corrections in the self-energy. As remarked in Ref. 31, the different levels of approximation for vertexes and single-particle Green's functions may then lead to unphysical results for the pseudogap in the spectral function, in a similar way to what happens for the 2D repulsive Hubbard model.<sup>38</sup> The important point to be emphasized is that, provided  $G^{(0)}$  in Eqs. (1) and (2) contains the dressed chemical potential obtained from Eqs. (3) and (4), this set of equations interpolates smoothly between weak- and strong-coupling limits and provides a reasonable description of both limits. A comparison between our results for the continuum model and those available for the lattice model will be made in Sec. VI, with the outcome that the main qualitative features remain the same in the two models.

### III. PAIRING FLUCTUATIONS FROM WEAK TO STRONG COUPLING

In this section, a systematic study of the crossover from the superconducting fluctuation (weak-coupling) regime to

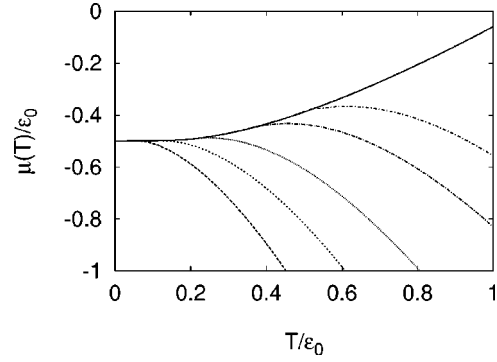


FIG. 1. Critical chemical potential  $\mu_c(T_c)$  (full line) and normal-phase chemical potential  $\mu(n, T)$  for different values of the density expressed in terms of  $(k_F a_F)^{-1}$  (broken lines), as functions of temperature. The values of  $(k_F a_F)^{-1}$  are 1.33, 0.96, 0.76, 0.60, and 0.52 from bottom to top.

the bosonic (strong-coupling) regime for the pair-fluctuation propagator is reported via both analytical and numerical calculations, for a wide temperature range above  $T_c$ . This study is preliminary to the discussion of the spectral function via the self-energy (1), presented in the next section.

The pair-fluctuation propagator  $\Gamma^{(0)}(\mathbf{q}, \Omega_\nu)$  within the non-self-consistent  $t$ -matrix approximation is given by Eq. (2). We shall examine, in particular, its wave vector and frequency dependence for all coupling regimes.

Being interested in *normal-phase* properties of the fermionic system, knowledge of the superconducting critical temperature  $T_c$  is required at the outset to insure that  $T \geq T_c$ . To identify the critical temperature  $T_c$ , we rely on the condition that the fluctuation propagator has a pole at  $T_c$  for vanishing wave vector and frequency, namely,  $\Gamma^{(0)-1}(\mathbf{q}=0, \Omega_\nu=0; \mu, T=T_c)=0$ . This condition (known as the Thouless criterion) taken alone is equivalent to the BCS equation for the critical temperature in the weak-coupling limit. In addition, when coupled to the density equation (4) to fix the chemical potential, it yields the value of the Bose-Einstein condensation temperature in the strong-coupling limit.

The Thouless criterion provides a temperature-dependent *critical value* for the chemical potential  $\mu_c(T_c) = \mu(n, T_c)$ , with  $\mu(n, T)$  obtained from the density equation. In Fig. 1 the critical chemical potential and the normal-phase chemical potential are reported for different values of  $(k_F a_F)^{-1}$  in the strong- to intermediate-coupling regime. We have verified that in the high-temperature limit the chemical potential  $\mu(n, T)$  tends to its classical value  $\mu(n, T) = 1.5T \ln(1.898T_{\text{BE}}/T)$  for all densities ( $T_{\text{BE}} = 3.31n_B^{2/3}/m_B$  being the Bose-Einstein condensation temperature).<sup>39</sup> Note that in the strong-coupling regime, i.e., at low density and for  $\beta|\mu| \gg 1$ ,  $\mu$  approaches the value  $-\epsilon_0/2$ , where  $\epsilon_0 = (ma_F^2)^{-1}$  is the binding energy of the associated two-body problem. In the intermediate-coupling regime,  $\mu$  initially increases as the temperature is increased, reaches a maximum, and eventually decreases, tending to the classical behavior. The temperature where the maximum is located turns out to be smaller than the binding energy  $\epsilon_0$  and does not relate to specific changes of single-particle properties in the strong- or

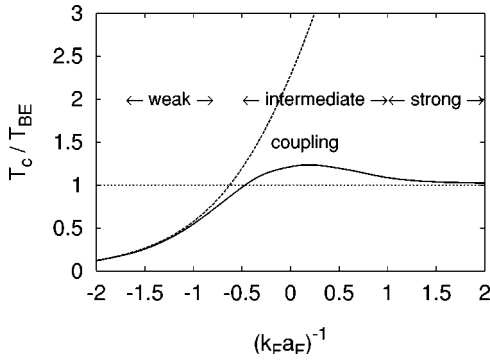


FIG. 2. Critical temperature  $T_c$  (full line) and BCS mean-field critical temperature  $T_{\text{BCS}}$  (broken line) as functions of  $(k_F a_F)^{-1}$  (both temperatures are normalized to the Bose-Einstein condensation temperature  $T_{\text{BE}}$  evaluated at the same density).

intermediate-coupling regimes. In the weak-coupling regime, on the other hand, this temperature turns out to coincide with the crossover temperature  $T^*$  where pair fluctuations become manifest and a pseudogap opens.

In the intermediate- and weak-coupling regime, the presence of the maximum in  $\mu(T)$  is connected with the fermionic degrees of freedom, and in particular with the opening of a pseudogap at the Fermi surface which tends to depress the chemical potential upon lowering the temperature (in a similar fashion to what happens when a real gap opens in a BCS superconductor below  $T_c$ ). In the weak-coupling regime, the temperature interval where the pseudogap is finite is very narrow and the maximum of  $\mu(T)$  approaches the critical line  $\mu_c(T_c)$ , becoming in practice not visible both in our results and in Monte Carlo simulations. The presence of a maximum of  $\mu(T)$  [with the ensuing nonmonotonic behavior of  $\mu(T)$ ] is clearly observed in Monte Carlo simulations of the 2D attractive ( $s$ -wave) Hubbard model in the intermediate-coupling regime (see Fig. 6 of Ref. 29), while the presence of the maximum is somewhat debated when the self-consistent  $t$ -matrix approximation is used.<sup>28,40</sup> In the strong-coupling regime, the fermionic degrees of freedom are exponentially suppressed according to  $f(\xi) \sim \exp(-\beta|\mu|)$  and the above maximum is progressively shifted toward zero temperature for increasing  $\beta|\mu|$ , thus recovering in the extreme strong-coupling limit the behavior of a free Bose gas via the relation  $2\mu = -\epsilon_0 + \mu_B$ .<sup>41,42,8</sup> We have verified that in the strong- and intermediate-coupling regimes, the temperature at which  $\mu(T)$  reaches its maximum does not relate with the temperature at which the pseudogap opens.

The equation for the density, together with the condition for the critical chemical potential  $\mu(T) = \mu_c(T)$ , yields the value of the critical temperature  $T_c$  for the superconducting instability. The critical temperature  $T_c$  and the BCS mean-field critical temperature  $T_{\text{BCS}}$  [the latter obtained formally from the same equations defining  $T_c$  but with the bare single-particle Green's function  $G^{(0)}$  replacing  $G$  in Eq. (4)] are reported in Fig. 2 as functions of the parameter  $(k_F a_F)^{-1}$  [recall that in the weak-coupling limit  $T_{\text{BCS}} = 1.67\epsilon_F \exp(\pi/2k_F a_F)$  ( $a_F < 0$ )]. (Both temperatures have been conveniently normalized to the Bose-Einstein conden-

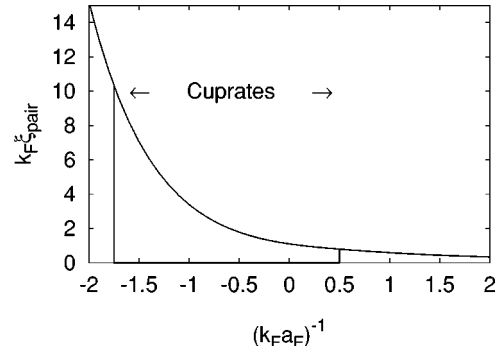


FIG. 3. Phenomenological parameter  $k_F \xi_{\text{pair}}$  as a function of the coupling parameter  $(k_F a_F)^{-1}$ , from weak to strong coupling.

sation temperature  $T_{\text{BE}}$  evaluated at the same density. Note that in the 3D continuum model  $T_{\text{BE}}$  is of the same order of  $\epsilon_F$ .) The results of Fig. 2 can be compared with the calculation of  $T_c$  within the non-self-consistent  $t$ -matrix approximation reported in Ref. 41. We mention that the inclusion of the self-energy shift  $\Sigma_0$  in the weak- to intermediate-coupling regime adopted in the present paper, slightly increases the value of the critical temperature with respect to the results of Ref. 41. We have verified that, in the strong- and intermediate-coupling regimes, the mean-field temperature  $T_{\text{BCS}}$  about coincides with the temperature at which the bare (fermionic) contribution  $n_0$  to the total density  $n$  equals the (bosonic) contribution  $\delta n$  due to interaction effects, i.e.,  $n_0(T = T_{\text{BCS}}) \approx \delta n(T = T_{\text{BCS}}) \approx n/2$ . This result permits us to identify  $T_{\text{BCS}}$  as the crossover temperature where preformed pairs start to form. [The connection between  $T_{\text{BCS}}$  and the characteristic crossover temperature(s) of the spectral function will be made in Sec. IV.] Note from Fig. 2 that for  $(k_F a_F)^{-1} \lesssim -1$  the critical temperature approaches the BCS mean-field critical temperature, indicating that the fermionic system is in the weak-coupling regime. For  $(k_F a_F)^{-1} \gtrsim 1$  the critical temperature is instead close to the Bose-Einstein condensation temperature, indicating that in the strong-coupling regime the fermionic system is equivalent to a system of noninteracting bosons. The strong-coupling limit is thus effectively reached for not too large values of the parameter  $(k_F a_F)^{-1}$ .<sup>43</sup>

In Fig. 3 we report for convenience the relation between  $k_F \xi_{\text{pair}}$  and  $(k_F a_F)^{-1}$  as obtained from the analytic solution of Ref. 44,  $\xi_{\text{pair}}$  being the average pair size at  $T=0$ . This plot is especially useful to compare our results for the two- and single-particle properties] which are expressed in terms of  $(k_F a_F)^{-1}$  with the phenomenology of cuprates, for which some estimates of the parameter  $k_F \xi_{\text{pair}}$  in different doping regimes are available<sup>7</sup>. Specifically, at optimum doping the parameter  $k_F \xi_{\text{pair}}$  takes roughly values between 6 and 10, and its value decreases for decreasing doping (mainly because the superconducting gap at  $T=0$  increases and the Fermi energy decreases approaching the insulating phase). We may reasonably consider  $k_F \xi_{\text{pair}} \approx 1$  as a lower-bound value for underdoped cuprates, especially if we consider it as a local quantity about the  $M$  points. Accordingly, the coupling parameter  $(k_F a_F)^{-1}$  in the optimum and underdoped regimes for cuprates lies approximately in the range  $-1.7$

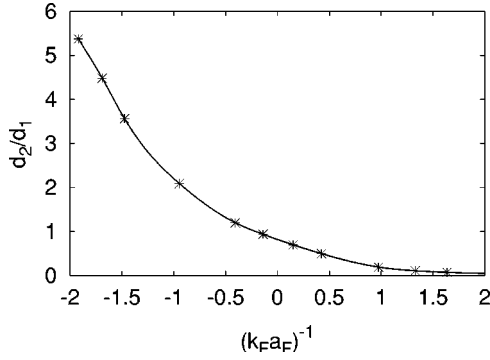


FIG. 4. Ratio between the imaginary ( $d_2$ ) and real ( $d_1$ ) part of the frequency coefficient of the inverse pair-fluctuation propagator at  $T_c$  as a function of  $(k_F a_F)^{-1}$ .

$\leq (k_F a_F)^{-1} \leq 0.5$ , as indicated in Fig. 3.

Having determined the thermodynamic quantities  $\mu(n, T)$  and  $T_c$ , we pass now to calculate the pair-fluctuation propagator (2). From a physical point of view, pairing fluctuations have essentially different character in the strong- and weak-coupling regimes. While to evaluate the self-energy numerically from Eq. (5) knowledge of  $\Gamma^{(0)}$  is required over a wide range of wave vectors and frequencies, to characterize the evolution of  $\Gamma^{(0)}$  from weak to strong coupling it is sufficient to consider the expansion of its inverse in powers of the wave vector  $\mathbf{q}$  and the Matsubara frequency  $\Omega_\nu$ :<sup>17,19</sup>

$$\Gamma^{(0)-1}(\mathbf{q}, \Omega_\nu) = a + b|\mathbf{q}|^2 + di\Omega_\nu \quad (8)$$

with  $d = d_1 + id_2 \text{sgn}(\Omega_\nu)$ . Here,  $(a, b, d_1, d_2)$  are real coefficients which are coupling, density, and temperature dependent.

In Fig. 4 we report the ratio of the imaginary ( $d_2$ ) to the real ( $d_1$ ) part of the frequency coefficient in Eq. (8) at  $T_c$  as a function of  $(k_F a_F)^{-1}$ . In the strong-coupling limit,  $d_1 \approx -m^2 a_F / (8\pi)$  and  $d_2 \approx 0$ , with the pair-fluctuation propagator acquiring the polar structure of a bosonic Green's function. In the weak-coupling limit, on the other hand,  $d_1 \approx -(T_c/E_F)^2 \ll 1$  and  $d_2 = -N_0 \pi / (8T_c)$ , where  $N_0$  is the density of states (per spin component) at the Fermi energy  $E_F$ , with the pair-fluctuation propagator acquiring the diffusive Ginzburg-Landau structure.<sup>34</sup> When  $|d_1| > |d_2|$ , fluctuating pairs become propagating (albeit with a damping), and eventually acquire the (bosonic) character of undamped preformed pairs.

In Fig. 5 the coefficient  $b$  of the  $|\mathbf{q}|^2$  term in Eq. (8) is plotted as a function of  $(k_F a_F)^{-1}$ . In the strong-coupling regime [i.e., for  $(k_F a_F)^{-1} \geq 1$ ],  $b$  coincides with its strong-coupling value  $ma_F / (32\pi)$ , where  $2m$  is the mass of the composite boson. In the weak-coupling regime (i.e., for  $1/k_F a_F \leq -1$ ),  $b = N_0 7 \zeta(3) v_F^2 / (48\pi^2 T_c^2)$  is proportional to the square of the zero-temperature correlation length  $\xi_0$  [where  $v_F$  is the Fermi velocity and  $\zeta(3) \approx 1.202$  is the Riemann zeta function of argument 3], and tends to diverge in the extreme weak-coupling limit.

Finally, the coefficient  $a$  in Eq. (8) provides a mass to the pair-fluctuation propagator. In the weak-coupling limit  $a = N_0 \ln(T/T_c)$  vanishes at  $T_c$ , while in the strong-coupling

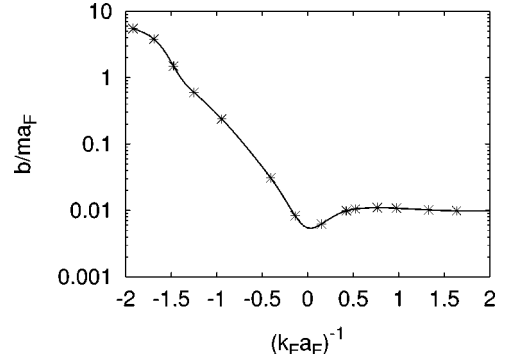


FIG. 5. Coefficient  $b$  of the  $|\mathbf{q}|^2$  term in the inverse pair-fluctuation propagator at  $T = T_c$  as a function of  $(k_F a_F)^{-1}$ .

limit we can write  $a = -m^2 a_F \mu_B(T) / (8\pi)$ , where  $\mu_B(T)$  is the bosonic chemical potential, which we pass now to discuss.

According to the above analysis, we have verified that in the strong-coupling regime (when the conditions  $\mu < 0$  and  $\beta|\mu| \gg 1$  are satisfied) the pair-fluctuation propagator evaluated numerically acquires the polar structure of a free-boson Green's function<sup>42,33</sup>

$$\Gamma^{(0)}(\mathbf{q}, \Omega_\nu) = -\frac{8\pi / (m^2 a_F)}{i\Omega_\nu - q^2 / (4m) + \mu_B} \quad (9)$$

with mass  $2m$ , a quadratic dispersion as a function of wave vector, and bosonic chemical potential  $\mu_B(T)$ , which reduces to  $2\mu(T) + \epsilon_0$  in the extreme strong-coupling limit. This implies that, for real frequencies, the imaginary part of  $\Gamma^{(0)}$  [which enters the calculation of the imaginary part of the self-energy via Eq. (5)] is proportional to a delta function in the strong-coupling limit

$$\text{Im} \Gamma^{(0)}(\mathbf{q}, \omega) = \frac{8\pi^2}{m^2 a_F} \delta[\omega - q^2 / (4m) + \mu_B]. \quad (10)$$

We have verified that Eq. (10) remains approximately valid in the intermediate-coupling regime toward strong coupling (when  $\beta|\mu| \sim 1$  and  $\mu < 0$ ), while only in the strong-coupling limit  $\mu_B(T)$  therein reduces to the chemical potential  $\mu_0(T)$  of an ideal Bose gas, with the characteristic temperature dependence

$$\mu_0(T) = -1.22 \frac{(T - T_{BE})^2}{T_{BE}} \quad (11)$$

at low enough temperature. Specifically, we have verified that a  $\delta$ -function contribution to  $\text{Im} \Gamma^{(0)}(\mathbf{q}, \omega)$  appears when  $(k_F a_F)^{-1} \geq 0$  (corresponding to  $d_2/d_1 \leq 1$  in Fig. 4). This contribution, which is initially present for large values of  $\mathbf{q}$ , extends progressively to smaller values of  $\mathbf{q}$  for increasing coupling, reaching eventually  $\mathbf{q} = 0$  when the chemical potential becomes negative. By further increasing the coupling, the  $\delta$ -function contribution to  $\text{Im} \Gamma^{(0)}(\mathbf{q}, \omega)$  becomes increasingly prominent and the asymptotic expression (10) is progressively reached.

This  $\delta$ -function contribution, associated with the formation of a bound state with bosonic character, is responsible in the strong-coupling limit for the opening of a real gap in a broad temperature range above  $T_c$ , as it will be shown in the next section. Actually, in addition to the  $\delta$  function, one also finds a finite contribution to  $\text{Im}\Gamma^{(0)}$  for  $\omega > 2|\mu|$ . When inserted in Eq. (5), this contribution leads to an exponentially vanishing  $\text{Im}\Sigma$  for  $\omega > |\mu|$ .

Finally, in the *weak-coupling* regime, the pair-fluctuation propagator recovers the Ginzburg-Landau diffusive form. Near the critical temperature, its expression for small wave vectors and frequencies is accordingly given by

$$\Gamma^{(0)}(\mathbf{q}, \Omega_\nu) = \frac{1}{N_0(\varepsilon + \eta|\mathbf{q}|^2 + \gamma|\Omega_\nu|)}. \quad (12)$$

Here,  $\varepsilon = \ln(T/T_c)$  is the mass term of the propagator,  $\eta \sim v_F^2/T_c^2$  represents the stiffness of the superconducting fluctuations with a proportionality coefficient which depends on dimensionality [ $7\zeta(3)/(48\pi^2)$  being its value in 3D], while  $\gamma = \pi/(8T_c)$  is related to the lifetime of the fluctuating pairs (which do not obey Bose statistics). In this limit,  $\text{Im}\Gamma^{(0)}(\mathbf{q} = 0, \omega)$  diverges as  $1/\omega$  only at the critical temperature  $T = T_c$ ; as a consequence, the pseudogap region induced by the diffusive pair fluctuations will be present only in a rather *narrow* temperature range. No delta function contributes in this regime, but  $\text{Im}\Gamma^{(0)}(\mathbf{q} = 0, \omega)$  has a broadened peak structure for small enough  $\mathbf{q}$ .

To summarize, the main effect of increasing coupling in  $\text{Im}\Gamma^{(0)}(\mathbf{q}, \omega)$  is the appearance of a peak structure (delta function) at finite frequencies, whose area grows with  $(k_F a_F)^{-1}$ . In the strong-coupling regime, for  $\mathbf{q} = 0$  and  $T > T_c$  the real part of  $\Gamma^{(0)}(\mathbf{q}, \omega)^{-1}$  vanishes at a finite frequency, corresponding to a pair resonance. This resonance disperses as  $\mathbf{q}^2$ . In the weak-coupling regime, the real part of  $\Gamma^{(0)}(\mathbf{q}, \omega)^{-1}$  is small only in the critical region, and vanishes only at the critical temperature. Increasing the coupling from weak to strong, the frequency dependence of  $\text{Im}\Gamma^{(0)}(\mathbf{q} = 0, \omega)$  evolves from being antisymmetric with respect to  $\omega = 0$  to an asymmetric structure. This evolution confirms previous results for  $\Gamma^{(0)}(\mathbf{q} = 0, \omega)$  reported in Ref. 17. In the next section, we will show how the peak structures of  $\Gamma^{(0)}(\mathbf{q}, \omega)$  affect the single-particle self-energy and hence the spectral function, giving rise to a (pronounced) suppression of the low-energy spectral weight, namely, to a pseudogap.

#### IV. SPECTRAL FUNCTION FROM WEAK TO STRONG COUPLING

In this section, we study the single-particle excitations for fermions coupled to pair fluctuations above the critical temperature. The spectral function  $A(\mathbf{k}, \omega)$ , obtained by solving the set of equations (1)–(7), is analyzed in a *systematic* way as a function of coupling and temperature, thus following its evolution from weak to strong coupling. In this way, characteristic features of the spectral function as a function of frequency and temperature will be evidenced in *all* coupling regimes. We shall analyze separately the cases when the chemical potential lies below the bottom of the single-

particle band ( $\mu < 0$ ) corresponding to the strong- to intermediate-coupling regime, and when the chemical potential lies inside the single-particle band ( $\mu > 0$ ) corresponding to the intermediate- to weak-coupling regime.

##### A. Strong- to intermediate-coupling regime

In the previous section, we have verified that a delta function appears in  $\text{Im}\Gamma^{(0)}(\mathbf{q}, \omega)$  starting from the intermediate-coupling regime when  $(k_F a_F)^{-1} > 0$  (for temperatures such that  $\beta|\mu| \geq 1$ ). In particular, we have verified that in the strong-coupling limit (where  $\mu < 0$  and  $\beta|\mu| \gg 1$ ) the pair-fluctuation propagator coincides with a free-boson Green's function with mass  $2m$  [see Eq. (9)]. In this limit, the imaginary part of the pair-fluctuation propagator reduces to a delta function and the self-energy can be evaluated analytically. Inserting Eq. (10) into the general expression (5) for the imaginary part of the self-energy, the following form results:

$$\text{Im}\Sigma(\mathbf{k} = 0, \omega) = \frac{-2(4m)^{3/2} \sqrt{\omega_{\text{th}} - \omega} \Theta(\omega_{\text{th}} - \omega)}{m^2 a_F e^{\beta(\omega_{\text{th}} - \omega + |\mu_B|)} - 1}, \quad (13)$$

where  $\omega_{\text{th}} = \mu - \mu_B$  is a threshold frequency and  $\Theta$  is the unit step function. [In the strong- to intermediate-coupling regime, when the chemical potential is below the bottom of the free-fermion band ( $\mu < 0$ ) and  $\mathbf{k}^2/(2m) \ll \epsilon_0$ , the self-energy and hence the spectral function are almost independent of wave vector. In this case,  $\mathbf{k} = 0$  can be taken as a representative value, as we did in Eq. (13).]

Note that the frequency dependence of  $\text{Im}\Sigma$  is strongly *asymmetric* about its minimum at  $\omega \approx \omega_{\text{th}} - |\mu_B|$ . Note also that  $\text{Im}\Sigma$  (and hence  $\text{Re}\Sigma$  obtained via Kramers-Kronig transform) has a nontrivial temperature and frequency dependence, showing strong deviations from Fermi-liquid behavior. In the regime where  $\beta|\mu_B| \ll 1$  (i.e.,  $T \approx T_c$ ), three different behaviors of  $\text{Im}\Sigma(0, \omega)$  can be specifically identified on the frequency axis: (i) For  $\omega_{\text{th}} - |\mu_B| < \omega < \omega_{\text{th}}$ ,  $\text{Im}\Sigma(0, \omega) \sim -\sqrt{\omega_{\text{th}} - \omega}/\beta|\mu_B|$  and (ii) for  $\omega_{\text{th}} - \beta < \omega < \omega_{\text{th}} - |\mu_B|$ ,  $\text{Im}\Sigma(0, \omega) \sim -(\beta\sqrt{\omega_{\text{th}} - \omega})^{-1}$ , and (iii) for  $\omega < \omega_{\text{th}} - \beta$ ,  $\text{Im}\Sigma(0, \omega) \sim -\exp[-\beta(\omega_{\text{th}} - \omega)]$ . Note that, in the strong-coupling limit, the imaginary part of the self-energy has a square-root divergence at  $\omega = \omega_{\text{th}}$  for  $T = T_c$ .

We have further verified numerically that strong deviations from Fermi-liquid behavior are present in the strong- to intermediate-coupling regime in a wide temperature range above  $T_c$  (while in the weak-coupling regime non-Fermi-liquid behavior is found only in a narrow temperature range above  $T_c$ , as discussed in the next subsection).

The above characteristic features of the analytic expression (13) can be clearly identified in the numerical results for  $\text{Im}\Sigma(\mathbf{k} = 0, \omega)$  reported in Fig. 6 at different temperatures (for a specific coupling). The associated real part is shown in Fig. 7, where the straight lines  $\omega + \mu$  are also reported for the same temperatures (and coupling), with increasing temperature from top to bottom. At any temperature, the intersection of a given straight line with  $\text{Re}\Sigma(\mathbf{k} = 0, \omega)$  locates the position of the quasiparticle peak at  $\omega > 0$ .

Note that for temperatures close to  $T_c$ , three intersections occur, with the most left intersection giving rise to the inco-

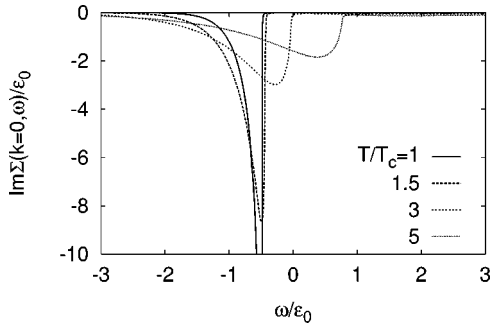


FIG. 6. Imaginary part of the self-energy at  $\mathbf{k}=0$  as a function of frequency (in units of  $\epsilon_0$ ) at different temperatures. In this case,  $(k_F a_F)^{-1}=0.77$  and  $T_c/T_{BE}=1.14$ . (Strong- to intermediate-coupling regime.)

herent peak in  $A(\mathbf{k}, \omega)$  at negative frequencies [while to the central intersection there corresponds a strong suppression of  $A(\mathbf{k}, \omega)$ ]. At high enough temperatures, on the other hand, only a single intersection occurs. The corresponding spectral function for the same coupling and temperatures above  $T_c$  is reported in Fig. 8. The resulting spectral function has a strongly asymmetric structure with two peaks: The one at positive frequencies is rather narrow, coherentlike, and has a large spectral weight (namely, the area enclosed by the peak); the one at negative frequencies is instead broad and has a small spectral weight. When the chemical potential  $\mu$  is below the bottom of the band, the peak located at negative frequencies represents the *incoherent peak* generated by the interaction of the fermions with strong pair fluctuations. This incoherent peak is itself asymmetric, it becomes broader for increasing temperature, its spectral weight is density and coupling dependent [decreasing as  $(k_F a_F)^3$ ], and its position depends mainly on the value of the chemical potential (which in turn depends on temperature). By increasing temperature, the chemical potential becomes progressively more negative (see Fig. 1) and the peak position of  $A(\mathbf{k}=\mathbf{0}, \omega)$  shifts accordingly toward positive frequencies. The broadening of the incoherent peak becomes pronounced when the temperature is of the order of the binding energy (see, e.g., the case with  $T/T_c=3$  in Fig. 8). Note also that, for increasing temperature, the two peaks in  $A(\mathbf{k}=\mathbf{0}, \omega)$  get broadened

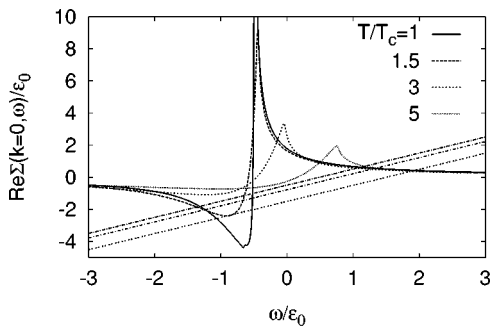


FIG. 7. Real part of the self-energy at  $\mathbf{k}=0$  as a function of frequency (in units of  $\epsilon_0$ ) at different temperatures. In this case,  $(k_F a_F)^{-1}=0.77$  and  $T_c/T_{BE}=1.14$ . (Strong- to intermediate-coupling regime.)

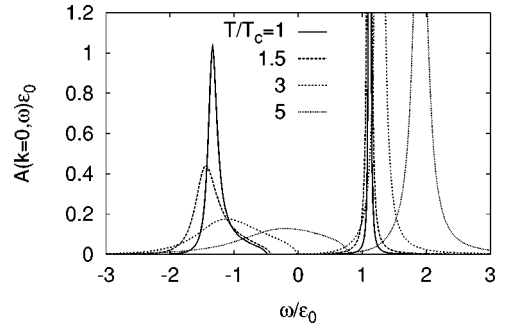


FIG. 8. Spectral function at  $\mathbf{k}=0$  as a function of frequency (in units of  $\epsilon_0$ ) at different temperatures. In this case,  $(k_F a_F)^{-1}=0.77$  and  $T_c/T_{BE}=1.14$ . (Strong- to intermediate-coupling regime.)

in an asymmetric way [in contrast to the weak-coupling regime (see below), approaching which the broadening of the two peaks becomes progressively more symmetric]. We have also verified that, in the extreme bosonic limit, the spectral function has the structure of two deltalike peaks symmetrically located with respect to  $\omega=0$  (albeit with quite different spectral weights), which is generated in an asymmetric way by the narrowing of the incoherent peak at negative frequencies as the product  $k_F a_F$  becomes smaller and smaller.

In Fig. 9 the spectral function at  $\mathbf{k}=\mathbf{0}$  is plotted as a function of frequency for different values of the parameter  $(k_F a_F)^{-1}$  at  $T=T_c$ . Note that these curves have been expressed in units  $\epsilon_F$ , instead of  $\epsilon_0$ , to get a more evident evolution with coupling. The spectral function has two well-separated peaks, with a *real gap* opening at an energy of the order of the binding energy of the pairs. By increasing the coupling, the spectral weight inside the gap is progressively suppressed, until in the extreme strong-coupling limit the step function in the imaginary part of the self-energy (13) makes the spectral weight to vanish identically in the range  $-|\mu| + |\mu_B| < \omega < |\mu|$ .

Since photoemission experiments measure the intensity of photoemitted electrons (that is, the spectral weight at *negative* frequencies), no signal would be detected if both the incoherent and coherent peaks had moved to positive frequencies for increasing temperature. In this context (and in analogy with what is empirically done when interpreting

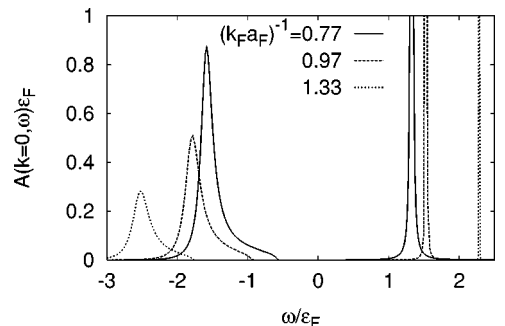


FIG. 9. Spectral function at  $\mathbf{k}=0$  as a function of frequency (in units of  $\epsilon_F$ ) at  $T=T_c$  for different values of the coupling  $(k_F a_F)^{-1}$ . (Strong- to intermediate-coupling regime.)

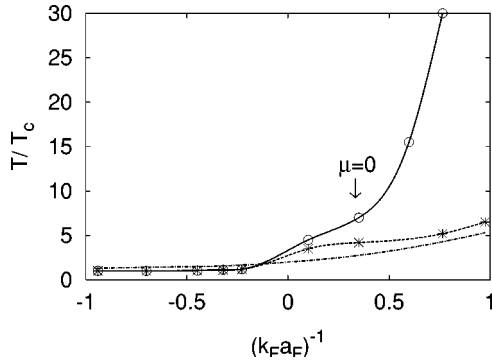


FIG. 10. Crossover temperatures  $T_0^*$  (dashed line) and  $T_1^*$  (full line), and BCS critical temperature  $T_{\text{BCS}}$  (dashed-dotted line) as functions of  $(k_F a_F)^{-1}$ ; all temperatures are normalized to the critical temperature  $T_c$  of Fig. 2. The value of  $(k_F a_F)^{-1}$  where the chemical potential changes sign is indicated by an arrow.

photoemission measurements), it is natural to introduce a crossover temperature  $T_0^*$  at which the maximum of the lower peak crosses zero frequency. Our analysis shows, however, that at  $T_0^*$  the spectral function still maintains a two-peak structure (see Fig. 8), reflecting the sizable effects of the interaction between fermions and pair fluctuations. We are accordingly led to introduce a second crossover temperature  $T_1^* > T_0^*$ , at which the upper and lower peaks of the spectral function merge just in one peak [in the sense that the incoherent peak is progressively absorbed by the coherent (quasiparticle) peak, even though the separation between the two peaks remains almost constant].

In Fig. 10 the two crossover temperatures  $T_0^*$  and  $T_1^*$  (as obtained numerically from the above definitions) are reported as functions of the parameter  $(k_F a_F)^{-1}$ , both temperatures being normalized with respect to the critical temperature  $T_c$ . The BCS mean-field critical temperature  $T_{\text{BCS}}$  from Fig. 2 is also reported for comparison. In the strong-coupling limit [when  $(k_F a_F)^{-1} \geq 1$ ]  $T_1^* \gg T_0^*$ ,  $T_1^*$  being a large energy scale which, according to Fig. 10, in the strong-coupling limit is much larger than the binding energy  $\epsilon_0$ . The difference between  $T_1^*$  and  $T_0^*$  is reduced by decreasing  $(k_F a_F)^{-1}$ , but only in the intermediate-coupling regime [i.e., when  $(k_F a_F)^{-1} \leq -0.1$ ] the two crossover temperatures almost coincide ( $T_1^* \approx T_0^*$ ). In the weak-coupling regime, only a single crossover temperature can be identified ( $T_1^* = T_0^*$ ), since in this regime the chemical potential is almost equal to the Fermi energy and the two peaks of the spectral function are symmetrically located about zero frequency. Note finally that  $T_0^*$  about coincides with  $T_{\text{BCS}}$  which was previously identified via an independent procedure. (When  $T_0^* \approx T_1^*$  we shall indicate both temperatures simply as  $T^*$ .)

### B. Intermediate- to weak-coupling regime

In the intermediate to weak-coupling regime, it becomes essential to take explicit account of the constant shift  $\Sigma_0$  introduced in Sec. II. This shift has been identified with the value of the real part of the self-energy (1) taken at the wave vector  $k_{\mu'}$  [such that  $\xi(k_{\mu'}) = 0$  and where the pseudogap

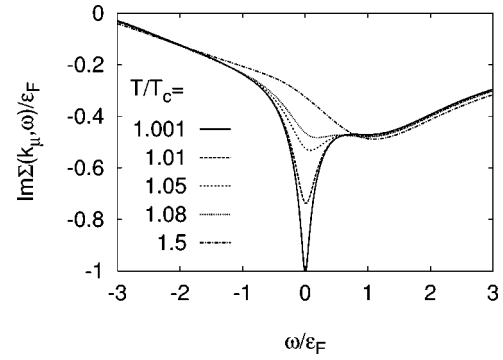


FIG. 11. Imaginary part of the self-energy at  $|\mathbf{k}| = k_{\mu'}$  as a function of frequency (in units of  $\epsilon_F$ ) at different temperatures when  $(k_F a_F)^{-1} = -0.45$  ( $T_c / \epsilon_F = 0.23$ ). (Intermediate- to weak-coupling regime.)

turns out to be minimal], at zero frequency (about which the relevant range of the pseudogap phenomena is centered), and at a temperature close to  $T^*$  (where the system recovers a Fermi-liquid behavior). An exact selection of  $T$  is, in practice, not required since  $\Sigma_0$  turns out to depend rather weakly on  $T$  in the intermediate- to weak-coupling regime. In this sense, we interpret  $\Sigma_0$  as a kind of Hartree shift, even though for our choice of the potential the true Hartree shift vanishes identically. We have consistently evaluated the constant shift  $\Sigma_0$  at  $|\mathbf{k}| = k_{\mu'}$ ,  $\omega = 0$ , and at the same temperature where the self-energy  $\Sigma(\mathbf{k}, \omega)$  of Eq. (1) is calculated.<sup>45</sup>

The inclusion of the above constant shift  $\Sigma_0$  stems from the need of improving the single-particle Green's functions entering the construction of the self-energy (1) when approaching  $T_c$ , only close to which pseudogap phenomena become appreciable in the intermediate- to weak-coupling regime. The choice of the self-energy (1) takes, in fact, into account fluctuation corrections only at the lowest order, a procedure which is certainly not completely satisfactory when approaching the critical temperature where all sort of fluctuation corrections become important. To approach  $T_c$ , one may try to improve the self-energy (1) by dressing the single-particle Green's functions therein with a constant self-energy insertion appropriate to the noncritical (temperature) region. On the other hand, the inclusion of the full self-consistent Green's function (without vertex corrections, however) leads to an overall depression of pseudogap phenomena and is not theoretically justified.<sup>31,33</sup> From a pragmatic point of view, we have verified that in the intermediate- to weak-coupling regime the pseudogap would open at negative frequencies (and not at  $\omega = 0$ , as expected from a simple physical intuition), if the constant self-energy shift  $\Sigma_0$  were not properly included. The pseudogap opening at negative frequencies would, in turn, be in contrast with Monte Carlo results and experimental findings.

The characteristic behavior of the imaginary and real parts of the self-energy at  $|\mathbf{k}| = k_{\mu'}$  are shown in Figs. 11 and 12, respectively, at different temperatures (for a given coupling). Note that the convexity of the curves  $\text{Im} \Sigma(k_{\mu'}, \omega)$  about  $\omega = 0$  is inverted with respect to the Fermi-liquid behavior, implying strong deviations from Fermi-liquid behavior also at moderate values of the coupling (i.e., such that a bound-

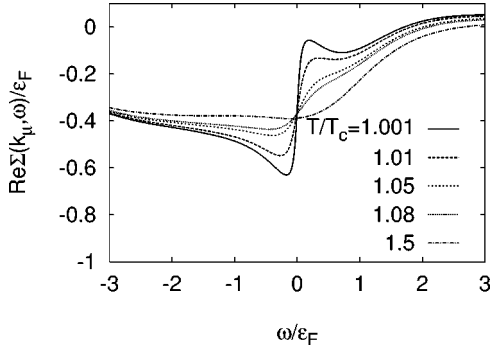


FIG. 12. Real part of the self-energy at  $|\mathbf{k}|=k_\mu$ , as a function of frequency (in units of  $\epsilon_F$ ) at different temperatures when  $(k_F a_F)^{-1} = -0.45$  ( $T_c/\epsilon_F = 0.23$ ). (Intermediate- to weak-coupling regime.)

state in the two-body problem is not yet present). We have verified, however, that the Fermi liquid behavior is consistently recovered when the coupling is progressively decreased.

In the weak-coupling limit and for temperature close to  $T_c$ , an analytic approximation for the imaginary part of the self-energy can be obtained by inserting into Eq. (5) the weak-coupling expression of the pair-fluctuation propagator given by Eq. (12). At zero frequency and at the Fermi wave vector, the imaginary part of the self-energy acquires then the following expression in the limit  $T \rightarrow T_c$ :

$$\text{Im } \Sigma(\mathbf{k}_F, \omega=0) = \frac{6\pi^3}{7\zeta(3)} \left( \frac{T_c}{\epsilon_F} \right)^2 \frac{T_c}{2} \ln \left( \frac{T - T_c}{T_c} \right) \quad (14)$$

which *diverges* upon approaching  $T_c$  with a slow logarithmic rate. An expression analogous to Eq. (14) is also obtained at finite frequency (such that  $|\omega| \ll \epsilon_F$ ) and  $T = T_c$ , with the replacement of  $\ln[(T - T_c)/T_c]$  by  $\ln(|\omega|/\omega_c)$ , where  $\omega_c \ll \epsilon_F$  is a suitable cutoff frequency.

To test the validity of the above analytic approximations, we may consider, e.g., the case of Fig. 11 for  $T/T_c = 1.001$  and obtain from Eq. (14) the value  $\text{Im } \Sigma/\epsilon_F \approx -0.92$  for  $\omega = 0$ . This estimate is indeed in good agreement with the numerical result reported in Fig. 11 (see the full curve therein), for which  $\text{Im } \Sigma/\epsilon_F \approx -1$ . A fine-tuning of the temperature very close to  $T_c$  is, however, necessary to get a sizable increase of  $|\text{Im } \Sigma|$  due to the logarithmic divergence in Eq. (14). For instance, to double the above value a temperature  $(T - T_c)/T_c = 10^{-6}$  has to be reached. In the 3D model here considered, the divergence of  $\text{Im } \Sigma$  is therefore not numerically detectable for all practical purposes. In addition, to test the validity of the counterpart of Eq. (14) extended to finite frequency as explained above, we may consider the case of Fig. 11 for  $T/T_c = 1.001$  and two different frequencies, say,  $\omega_1/\epsilon_F = 0.075$  and  $\omega_2/\epsilon_F = 0.037$ . In this case, we obtain from our analytic approximation the value  $[\text{Im } \Sigma(\omega_1) - \text{Im } \Sigma(\omega_2)]/\epsilon_F = 0.093$ , which is rather close to the numerical result 0.106 as obtained from Fig. 11.

The analytic approximation (14) (as well as its counterpart at  $T = T_c$  and finite  $\omega$ ) need to be compared with the analytic form of  $\Sigma(\mathbf{k}, \omega)$  obtained in the weak-coupling limit

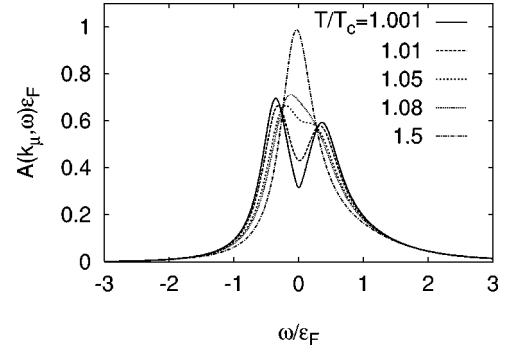


FIG. 13. Spectral function at  $|\mathbf{k}|=k_\mu$ , as a function of frequency (in units of  $\epsilon_F$ ) at different temperatures. In this case, with  $(k_F a_F)^{-1} = -0.45$  ( $T_c/\epsilon_F = 0.23$ ). (Intermediate- to weak-coupling regime.)

by Ref. 46 within the same non-self-consistent  $t$ -matrix approximation adopted in the present paper. According to Ref. 46, the diffusive form (12) of the pair-fluctuation propagator would yield

$$\Sigma(\mathbf{k}, \omega) = \frac{\Delta_{\text{pg}}^2}{\omega + \xi(\mathbf{k}) + i\gamma}, \quad (15)$$

where  $\Delta_{\text{pg}}$  is a parameter that depends on a wave-vector cutoff and  $\gamma \propto (T - T_c)$ . This expression evidently does not reduce to Eq. (14) for  $\omega = 0$  and  $T \rightarrow T_c$ , nor to the counterpart of Eq. (14) for  $T = T_c$  and finite  $\omega$ . A few comments to clarify the origin of these discrepancies are then in order.

The expression (15) has been derived more recently in Ref. 50, where it was also extensively used to fit ARPES data for Bi-based cuprates. According to Ref. 50, Eq. (15) results by manipulating directly the expression (1) for the self-energy in Matsubara frequency, whereby the finite value  $\pi T$  of the smallest (fermionic) Matsubara frequency is exploited to make approximations on the  $\mathbf{q}$  dependence of the integrand. Analytic continuation to the real frequency axis is then performed on the approximate result, eventually yielding expression (15) above. This procedure is, however, questionable, insofar as the very variable to be analytically continued is used to set restrictions on the approximate form of the function (in this case, the  $\mathbf{q}$  dependence of the integrand). In our procedure, on the other hand, analytic continuation is performed *at the outset* [see Eq. (5)] and the relevant (controlled) approximations to get the approximate result (14) are introduced only afterwards.

Note, in addition, that at  $|\mathbf{k}|=k_F$  the expression (15) produces two peaks symmetrically located about  $\omega = 0$ . This expression cannot, therefore, be used to fit the curves of  $A(k_\mu, \omega)$  for the coupling values we are considering (see Figs. 13 and 16 below), whereby the symmetry of the two peaks is recovered only in the extreme weak-coupling limit. In the analysis reported in Ref. 50, on the other hand, the experimental data are artificially symmetrized and the expression (15) (together with an additional scattering rate  $i\Gamma_1$ ) is used to fit the ARPES data. We shall propose below an alternative phenomenological fit to the curves of  $A(k_\mu, \omega)$ , which is suggested by our numerical calculations.

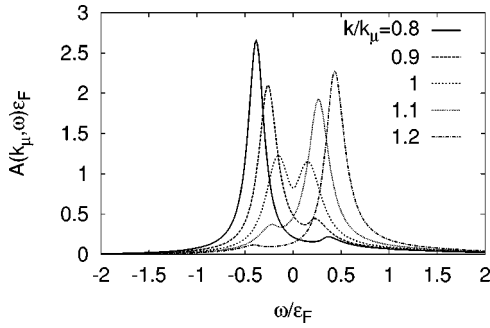


FIG. 14. Spectral function at different wave vectors  $|\mathbf{k}|$  about  $k_{\mu'}$ , as a function of frequency (in units of  $\epsilon_F$ ), for  $(k_F a_F)^{-1} = -0.72$  and  $T/T_c = 1.001$ . (Intermediate- to weak-coupling regime.)

In our numerical calculations we have found that, at low enough temperature, there are three intersections of the curves  $[\text{Re}\Sigma(k_{\mu'}, \omega) - \Sigma_0]$  with the straight line  $\omega$  (not shown in Fig. 12), with the two outer intersections giving rise to the two peaks of  $A(k_{\mu'}, \omega)$  (see Fig. 13) while the central intersection corresponds to a strong suppression of  $A(k_{\mu'}, \omega)$  owing to the associated large value of  $\text{Im}\Sigma(k_{\mu'}, \omega)$ . By increasing temperature, on the other hand, only one intersection remains [resulting in only one visible peak in  $A(k_{\mu'}, \omega)$ , see Fig. 13]. The associated spectral function at  $|\mathbf{k}| = k_{\mu'}$  is reported in Fig. 13 for the same temperatures and coupling of Figs. 11 and 12. The spectral function obtained in the intermediate-coupling regime shows a well-developed two-peak structure near  $T_c$  with a minimum at zero frequency; yet the spectral weight distribution remains slightly asymmetric about zero frequency, even when approaching the critical temperature. At zero frequency the spectral function has a sizeable finite value, indicating that no real gap opens at the Fermi surface. Note from Fig. 13 that, upon increasing the temperature, the pseudogap fills in and closes at the same time, with the two peaks of the spectral function merging in just one peak at a crossover temperature  $T_1^* \approx T_0^*$  (which in this particular case is between  $1.05T_c$  and  $1.08T_c$ ). It is thus apparent that a breakdown of the normal-state Fermi liquid occurs well before the system is in the preformed-pair limit. From the two-peak structure of  $A(k_{\mu'}, \omega)$  in the intermediate- to weak-coupling regime, a pseudogap  $\Delta_{\text{pg}}$  could be empirically defined either as *half* the frequency separation between the maxima of the peaks, or as the separation of the maximum of the lower peak (at negative frequencies) from zero frequency. These two definitions coincide in the weak-coupling limit but slightly differ in the strong-coupling limit (see also Table II below). Throughout this paper we will adopt the second definition, which is the most relevant for comparison with photoemission experiments, accessing only negative frequencies.

In the intermediate-coupling regime, when the chemical potential lies inside the fermion band and the Fermi surface is well defined, the wave-vector dependence of the spectral function shows a strong asymmetry about the wave vector  $k_{\mu'}$ . In Fig. 14 the spectral function is reported as a function of frequency for different wave vectors about  $k_{\mu'}$ , when  $T \approx T_c$ . It is clear from this figure that for  $|\mathbf{k}| < k_{\mu'}$ , a well-defined peak is found at negative frequencies, and that in-

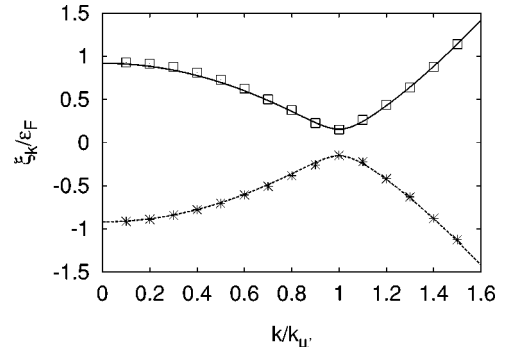


FIG. 15. Peak positions of the spectral function at negative (asterisks) and positive (squares) frequencies versus wave vector for  $(k_F a_F)^{-1} = -0.72$  and  $T/T_c = 1.001$ . Full and dotted lines represent the BCS-like fit. (Intermediate- to weak-coupling regime.)

creasing the wave vector to  $|\mathbf{k}| > k_{\mu'}$ , this peak becomes a small and broad incoherent peak. Thus, for  $|\mathbf{k}| < k_{\mu'}$ , the spectral weight of the coherent peak at negative frequencies decreases as the wave vector  $\mathbf{k}$  approaches  $k_{\mu'}$ , while at the same time the spectral weight of the associated incoherent peak located at positive frequencies increases, with a transfer of spectral weight from negative to positive frequencies upon crossing the “Fermi surface” (which is defined as the locus of minimum pseudogap, and almost coincides with the sphere  $k = k_{\mu'}$ ; note that for the coupling value of Fig. 14,  $k_{\mu'}$  is about 10% smaller than  $k_F$ ). This clearly shows that the interaction of the fermions with pair fluctuations gets increasingly stronger upon approaching the “Fermi surface,” so that deviations from the Fermi liquid picture appear to be stronger at low energy.

In Fig. 15 the positions of the two peaks of the spectral function are reported for different wave vectors about  $k_{\mu'}$ , when  $T \approx T_c$ . The results of our non-self-consistent  $t$ -matrix approximation (squares and asterisks) are here compared with the BCS-like dispersion  $\omega = \pm \sqrt{\xi(\mathbf{k})^2 + \Delta_{\text{pg}}^2}$  (continuous and dotted lines), where the BCS gap has been replaced by the pseudogap  $\Delta_{\text{pg}}$  at  $k_{\mu'}$ . It is rather remarkable that the coherent peak of the spectral function at  $|\mathbf{k}| < k_{\mu'}$ , gets reflected into the incoherent peak at  $|\mathbf{k}| > k_{\mu'}$ , as the wave vector crosses the “Fermi surface” (with the characteristic behavior of an avoided level crossing), in such a way that the position of the peak at negative frequencies follows almost exactly the BCS-like dispersion, provided the value of the pseudogap is inserted as explained above.

To fit the prominent features of  $A(k_{\mu'}, \omega)$  with a simple analytic expression [from which the corresponding form of  $\Sigma(k_{\mu'}, \omega)$  replacing Eq. (15) could be extracted], we may consider two Lorentians of width  $\gamma_L$  and  $\gamma_R$ , centered at  $-\Delta_L$  and  $\Delta_R$ , and with weights  $p_L$  and  $p_R$  (such that  $p_L + p_R = 1$ ), with the labels  $L$  and  $R$  referring to the left and right peaks of  $A(k_{\mu'}, \omega)$ , in the order. In Tables I and II we report the values of the fitting parameters  $\Delta_L$ ,  $\Delta_R$ ,  $\gamma_L$ ,  $\gamma_R$ , and  $\alpha = 1 - 2p_L$  for the curves of Fig. 13 (fixed coupling and varying temperature) and of Fig. 16 (fixed temperature and varying coupling), respectively.

Note that the asymmetry of the two Lorentians (which is controlled by the parameters  $\alpha$  and  $\gamma_L/\gamma_R$ ) is considerable,

TABLE I. Fitting parameters for the curves of Fig. 13. Energy variables are in units of  $\epsilon_F$ .

$T/T_c$	$\Delta_L$	$\Delta_R$	$\gamma_L$	$\gamma_R$	$\alpha$
1.001	0.31	0.31	0.16	0.29	0.22
1.01	0.28	0.28	0.17	0.32	0.28
1.05	0.21	0.21	0.18	0.33	0.33
1.08	0.18	0.18	0.18	0.34	0.36

increasing for increasing temperature or coupling (but for the last value of Table II). For temperatures and couplings larger than those reported in the tables, however, the fit of  $A(k_{\mu'}, \omega)$  with two Lorentzians become inadequate. Note also that in most cases  $\Delta_L = \Delta_R = \Delta_{pg}$ . In these cases a relatively simple form for  $\Sigma(k_{\mu'}, \omega)$  can be extracted, yielding

$$\Sigma(k_{\mu'}, \omega) = -i(\gamma - \alpha\delta) + \alpha\Delta_{pg} + \frac{(1 - \alpha^2)(\Delta_{pg}^2 - \delta^2) - 2i\Delta_{pg}\delta(1 + \alpha^2)}{\omega + \alpha\Delta_{pg} + i(\gamma + \alpha\delta)}, \quad (16)$$

where  $\gamma = (\gamma_R + \gamma_L)/2$  and  $\delta = (\gamma_R - \gamma_L)/2$ . Note that, even in the symmetric case with  $\alpha = 0$  and  $\delta = 0$ , the expression (16) does not reduce to the form (15) [due to the presence of an extra term  $-i\gamma$  in Eq. (16)], unless  $\Delta_{pg} \gg \gamma$  [this condition would be consistent with the assumptions under which Eq. (16) has been derived only when  $T$  approaches  $T_c$  (Ref. 46)]. However, the condition  $\Delta_{pg} \gg \gamma$  is never satisfied by our fits, where  $\Delta_{pg}$  and  $\gamma$  are of the same order.

In Fig. 16 the spectral function at  $|\mathbf{k}| = k_{\mu'}$  is reported for different values of  $(k_F a_F)^{-1}$  from intermediate to weak coupling, slightly above the critical temperature. Note that, in the weak-coupling regime, the spectral function acquires an almost symmetric two-peak structure, which differs from the standard BCS result at  $T = 0$  essentially for the broadening of the peaks due to the finite lifetime of the pairs. Note also that the pseudogap near the critical temperature decreases with coupling.

An analysis of the pseudogap opening within a 2D attractive Hubbard model in the weak-coupling regime has recently been reported in Ref. 37, by means of the non-self-consistent  $T$ -matrix approximation formulated on the real frequency axis. The frequency dependence of the spectral function obtained in that paper (at quarter filling) resembles the results of our Fig. 16.

TABLE II. Fitting parameters for the curves of Fig. 16. Energy variables are in units of  $\epsilon_F$ .

$(k_F a_F)^{-1}$	$\Delta_L$	$\Delta_R$	$\gamma_L$	$\gamma_R$	$\alpha$
-1.1	0.035	0.035	0.042	0.047	0.060
-0.72	0.14	0.14	0.11	0.15	0.17
-0.23	0.47	0.61	0.22	0.33	0.15
0	0.78	0.84	0.25	0.18	0.008

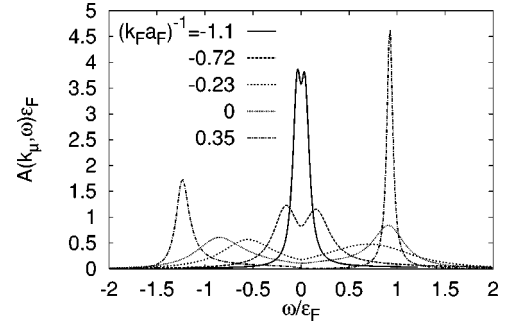


FIG. 16. Spectral function at  $|\mathbf{k}| = k_{\mu'}$  as a function of frequency  $\omega$  (in units of  $\epsilon_F$ ) for different values of  $(k_F a_F)^{-1}$  and  $T/T_c = 1.001$ . (Intermediate- to weak-coupling regime.)

Finally, a comparison of the pseudogap  $\Delta_{pg}$  at  $T_c$  with the BCS gap  $\Delta_{BCS}$  at  $T = 0$  and with the two-body gap  $\epsilon_0/2 = \epsilon_F / (k_F a_F)^2$  (which is nonvanishing only for  $a_F > 0$ ) is shown in Fig. 17 for all coupling regimes {when  $\mu < 0$ ,  $\Delta_{BCS}(T = 0)$  is set equal to  $[\mu^2 + \Delta(T = 0)^2]^{1/2}$ }. Note that in the weak-coupling limit  $\Delta_{pg}(T = T_c) \ll \Delta_{BCS}(T = 0)$ , while in the intermediate-coupling regime  $\Delta_{pg}(T = T_c) \approx \Delta_{BCS}(T = 0)$ . Moreover, in the intermediate- to strong-coupling regime (where  $a_F > 0$ ), both  $\Delta_{BCS}$  and  $\Delta_{pg}$  approach  $\epsilon_0/2$  from above as the coupling is increased. Many-body effects thus increase the pair-breaking energy scale with respect to the two-body limit. This result resembles the pair-size-shrinking effect noticed in Ref. 48 at the mean-field level.

In this context, it is interesting to mention that, taking  $\epsilon_F \approx 400$  meV as a representative value for cuprate superconductors, the range  $\Delta_{pg} \approx 20 - 120$  meV characteristic of cuprate superconductors corresponds to  $0.05 \leq \Delta_{pg}/\epsilon_F \leq 0.3$ , which (as seen from Fig. 17) lies within the range identified in Fig. 3 for cuprates.

### C. Criterion to distinguish weak from strong coupling

The above systematic study of the single-particle spectral function from weak to strong coupling suggests the following criterion to distinguish by ARPES experiments whether a fermion system with an attractive interaction lies in the strong- or weak-coupling regime. This criterion rests on the analysis of the spectral function at negative frequencies (just

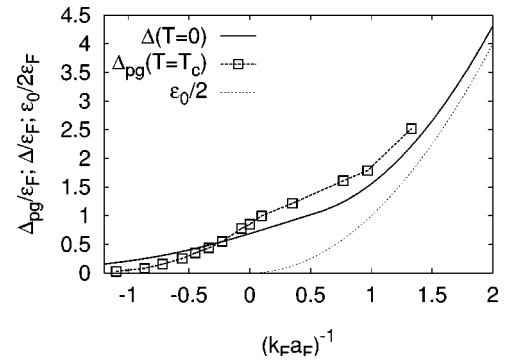


FIG. 17. Pseudogap at  $T = T_c$ , superconducting gap evaluated within the BCS approach at  $T = 0$  and gap in the strong-coupling limit, as functions of  $(k_F a_F)^{-1}$ .

as determined by ARPES experiments) for different values of the wave vector  $\mathbf{k}$ , and (as discussed in the next section) it is meant to be useful for interpreting the experimental data for cuprates in conjunction with the two-gap model mentioned in the Introduction.

Consider first a system in the intermediate- to weak-coupling regime, for temperatures between  $T^*$  and  $T_c$ , i.e., within the pseudogap region. In this case, the chemical potential lies inside the single-particle band and almost coincides with the Fermi energy. For wave vectors smaller than  $k_{\mu'}$ , the spectral function has a quasiparticle peak with large spectral weight at negative frequencies and a smaller incoherent peak at positive frequencies. Upon moving the wave vector across the ‘‘Fermi surface’’ ( $|\mathbf{k}| > k_{\mu'}$ ), the quasiparticle peak shifts toward positive frequencies, while the incoherent peak is now present at negative frequencies (see Fig. 14) and can accordingly be measured by ARPES. Restricting to negative frequencies and realizing a cut in wave vector space which probes the main and the reflected (shadow) bands, starting from  $|\mathbf{k}| < k_{\mu'}$ , ARPES should initially find a well-defined quasiparticle peak which, upon increasing the wave vector to  $|\mathbf{k}| > k_{\mu'}$ , should be reflected as a small and broad incoherent peak. Moreover, at  $|\mathbf{k}| = k_{\mu'}$ , the spectral weight at zero frequency remains a sizeable fraction of the peak maximum.

Consider then a system in the intermediate- to strong-coupling regime (when  $\mu < 0$ ), for temperatures between  $T_0^*$  and  $T_c$ . In this case, the chemical potential lies outside the single-particle band. For *any* wave vector, the spectral function has now a quasiparticle peak with large spectral weight at positive frequencies and a weaker incoherent peak at negative frequencies. For this reason, no appreciable difference in the shape of the spectral function should be detected by varying the wave vector. Thus, starting, e.g., from  $\mathbf{k} \equiv (k_x < 0, 0, 0)$  ARPES should find a broad incoherent peak which, upon increasing the wave vectors to  $(k_x > 0, 0, 0)$ , should not change appreciably. In addition, the spectral weight vanishes or is much less than the maximum of the incoherent peak in a range of frequencies of the order of the pseudogap (see Fig. 9).

By this token, it is clear that, for a fermionic system with an attractive interaction, the wave-vector dependence and the line shape of the spectral function at negative frequencies have well-pronounced qualitative differences depending on the coupling strength, differences which may be detected by a detailed ARPES analysis of the spectral function, as discussed next. Recall, however, that comparison of our results with ARPES data relies essentially on the two-gap model mentioned in the Introduction, and can be complicated by the presence of additional sources of quasiparticle scattering in cuprates as well as by the fact that the continuum model relates strong coupling to low density. Yet, our analysis can be useful to understand the evolution of the spectral properties along the Fermi surface.

## V. COMPARISON WITH ARPES SPECTRAL FUNCTION

The theoretical analysis of the spectral function from weak to strong coupling presented in this paper can be used

to analyze the spectral intensities measured by ARPES in Bi-based superconducting cuprates, for which a systematic experimental analysis is also available. In particular, we consider ARPES intensities measured in Bi2212 near the  $M$  points of the Brillouin zone as well as along the Fermi surface, moving from the  $M$  points toward the  $N$  (nodal) points, in different doping regimes and at different temperatures. According to our interpretation, the effective coupling between fermions should increase from the weak- to strong-coupling regime, when the doping is reduced from overdoping to underdoping. Moreover, as discussed in the Introduction, when moving from  $N$  toward  $M$  points along the Fermi surface, a continuous crossover from weakly to strongly coupled fermionic states should be observed even at fixed doping. We summarize the main results extracted from our work, which can be compared with ARPES experiments performed in Bi2212 materials.

### *Strong- to intermediate-coupling regime (about $M$ points).*

In the strong- to intermediate-coupling regime, where the chemical potential is below the bottom of the single-particle band, our results show that the spectral function displays two peaks, one incoherent at negative frequencies and the other one coherent at positive frequencies. In this case, the wave vectors are meant to be reckoned with respect to (one of) the  $M$  points. In this regime, the prominent features to be compared with experiments are as follows.

(i) The line shape of the spectral function at negative frequencies is quite broad, and the height of the incoherent peak noticeably decreases with increasing temperature (see Fig. 8) or increasing coupling (see Fig. 9). These features are in qualitative agreement with the behavior of the spectral intensity observed by ARPES in the pseudogap phase of underdoped cuprates, by decreasing doping and increasing temperature. Several ARPES measurements show, in fact, that the height of the peak in the spectral intensities collected about the  $M$  points decreases with underdoping, with heavily underdoped cuprates displaying a very broad structure with no detectable peak [see, e.g., Fig. 2 (left panel) of Ref. 47 and Fig. 1(a) of Ref. 2, for the doping dependence of the spectral weight about the  $M$  points]. ARPES measurements for the temperature dependence of the (quite broad) spectral intensities about the  $M$  points further indicate that the spectra are (slightly) suppressed for increasing temperature [see Fig. 2(b) of Ref. 2].

(ii) The spectral weight near zero frequency is strongly suppressed and a real gap opens in the spectral function in the strong-coupling regime (see Figs. 8 and 9). Experimental evidence for a strong suppression of the spectral weight near zero frequency can indeed be found, e.g., in Fig. 2 (left panel) of Ref. 47 for (heavily) underdoped samples with  $T_c = 56$  K.

*Intermediate- to weak-coupling regime (between  $M$  and  $N$  points).* In the intermediate- to weak-coupling regime, the chemical potential lies within the single-particle band and the wave vectors are referred to the center of the Brillouin zone. In this case, the salient features of our calculations to be compared with experiments are as follows.

(i) A single quasiparticle peak is present in the spectral function above the crossover temperature  $T^*$  (see Fig. 13),

implying a well-defined Fermi surface. Underdoped, optimally doped, and overdoped cuprates for wave vectors near the nodal points display quasiparticle peaks in the ARPES intensities (see, e.g., Fig. 1 of Ref. 49).

(ii) Approaching the critical temperature from above, the interaction between fermions and (damped) pair fluctuations determines a suppression of spectral weight near zero frequency and therefore the opening of a pseudogap, characterized by a finite spectral weight at zero frequency (see Fig. 13). In addition, the quasiparticle peak disperses as a function of the wave vector and, as the wave vector moves across the Fermi surface, is reflected as an incoherent broad peak (see Fig. 14). ARPES intensities in *underdoped* cuprates, measured about the  $N$  points for temperatures between  $T^*$  and  $T_c$ , display this feature, even though the reflection cannot be accurately identified (probably owing to the low spectral weight of the incoherent peak). In particular, a spectral weight suppression at low frequencies and a finite spectral weight at zero frequency has been found by ARPES [see, e.g., Fig. 1(b) and Fig. 3(a) of Ref. 50]. Experimental evidence for the reflection of the quasiparticle peak into an incoherent peak has also been found by ARPES measurements of the peak along the  $MY$  direction in the pseudogap phase of slightly underdoped cuprates [see Fig. 2(b) of Ref. 22], for which the intermediate- to weak-coupling regime should apply.

(iii) Increasing the coupling from the weak- to the intermediate-coupling regime, the pseudogap evaluated at  $T_c$  increases and the ratio between the pseudogap at  $T_c$  and the BCS gap evaluated at  $T=0$  also increases (see Fig. 17), about coinciding in the intermediate-to-strong coupling region. In all underdoped cuprates, and for any wave vector, the experimentally determined pseudogap at  $T_c$  clearly increases with decreasing doping, and in heavily underdoped cuprates it almost coincides with the superconducting gap measured at zero temperature [see, e.g., Fig. 3(b) of Ref. 2].

## VI. DISCUSSION AND CONCLUSIONS

In this paper, the evolution (from superconducting fluctuations to the bosonic limit) of the pseudogap opening and the spectral function has been studied in a *systematic way*. A system of fermions in a three-dimensional continuum, mutually interacting via an attractive contact potential, has been examined. In this way, the numerical calculation of the single-particle Green's function has been considerably simplified, yet preserving the main physical effects underlying the pseudogap opening. The pair-fluctuation propagator, the (one-loop) self-energy, and the spectral function have been evaluated as functions of coupling strength and temperature, from weak to strong coupling, and analytic and numerical results have been presented.

In the strong-coupling regime, the pair-fluctuation propagator has been shown to have bosonic character and the line shape of the incoherent peak of the spectral function to be strongly asymmetric about its maximum, with its spectral weight decreasing by increasing coupling (or decreasing density) and increasing temperature. In this regime, two crossover temperatures  $T_1^*$  (at which the two peaks in the spectral

function merge in just one peak) and  $T_0^*$  (at which the maximum of the incoherent peak crosses zero frequency) have been identified, with  $T_1^* > T_0^* \gg T_c$  and with  $T_0^*$  of the order of the binding energy of preformed pairs (ARPES experiments, however, can only measure  $T_0^*$ ).

In the intermediate-coupling regime, the line shape of the spectral function about the ‘‘Fermi surface’’ resembles the line shape of the spectral intensity (which is, in turn, related to the spectral function) measured by ARPES in underdoped cuprates between  $T_c$  and  $T^*$  for different wave vectors. In particular, we have reproduced the main features characterizing the ARPES pseudogap, namely, a finite spectral intensity at zero frequency and a finite pseudogap at  $T=T_c$  which is of the same order of the superconducting gap at zero temperature. We have also found that in the intermediate- to weak-coupling regime pseudogap effects are present only in a narrow temperature range above the critical temperature, a result related with the 3D character of the pair fluctuations (in 2D this temperature range should, in fact, be considerably wider).

In the weak-coupling regime, the pair fluctuation propagator acquires the diffusive Ginzburg-Landau character and the line shape of the spectral function gets progressively more symmetric as the coupling is decreased. In this regime, the two crossover temperatures  $T_1^*$  and  $T_0^*$  coincide and are of the order of  $T_c$ , with the pseudogap closing and filling-in quickly as the temperature is increased above  $T_c$ .

It is thus clear that the pseudogap already occurs in the one-loop approximation for the self-energy, namely, the non-self-consistent  $t$ -matrix approximation which we have adopted in this paper.

Maly *et al.* propose a (conserving) method to improve the non-self-consistent  $T$ -matrix approximation, by including the feedback effect of the self-energy in the two-particle propagator.<sup>17</sup> This is done by substituting in the particle-particle bubble one bare Green's function with a dressed one ( $G^0 G^0 \rightarrow G G^0$ ), following the approach by Kadanoff and Martin as extended by Patton.<sup>51</sup> These authors show that the consequence of the feedback on the self-energy is to enhance the resonance in the two-particle propagator found already by the lowest-order theory. However, by comparison of Maly *et al.* results with our (nonconserving) calculation (which includes although the Hartree-type self-energy shift  $\Sigma_0$ ), it turns out that the salient features of the spectral function are essentially preserved by the two calculations.

A similar non-self-consistent (as well as a self-consistent) calculation for the spectral function has been reported in Ref. 19. Specifically, even though Yanase and Yamada also make use of the non-self-consistent  $T$ -matrix approximation with  $d$ -wave pairing, their calculations are based on a small  $\mathbf{q}$  and  $\Omega$  expansion of the two-particle propagator while the chemical potential is kept at the Fermi level. As a consequence, the critical temperature evaluated by Yanase and Yamada coincides with the mean-field temperature  $T_{\text{BCS}}$ , which strongly deviates from  $T_c$  reported in our Fig. 2 in the intermediate- and strong-coupling regimes.

Most significantly, the results presented in this paper, concerning the temperature and wave-vector dependence of the

spectral function in the pseudogap phase, are in qualitative agreement with Monte Carlo simulations of the 2D attractive ( $s$ -wave) Hubbard model. In particular, in Refs. 30 and 31 the spectral function obtained by Monte Carlo simulations is reported in the intermediate-coupling regime for different temperatures and wave vectors. These simulations clearly show that in the pseudogap phase the spectral function has a two-peak structure, with the incoherent peak smoothly emerging from the main peak as the temperature is lowered below  $T^*$ . In addition, moving the wave vector across the Fermi surface, the main peak is reflected in a shadow incoherent peak, as reported in Ref. 29. Monte Carlo simulations thus give further support to our non-self-consistent  $t$ -matrix approximation, suggesting that dimensionality and lattice effects do not modify appreciably the main qualitative features of the pseudogap phase, obtained by our work for a 3D continuum with a contact potential.

Other kinds of fluctuation propagators (such as, charge-density wave,<sup>52,53</sup> spin-density wave,<sup>54–56</sup> and phase fluctuations above the Kosterlitz-Thouless transition<sup>25</sup>) result into peak structures in the two-particle Green's function and into an associated pseudogap opening in the single-particle spec-

tral function. In particular, the pioneering work by Kampf and Schrieffer<sup>55</sup> considering antiferromagnetic fluctuations coupled to fermions has shown that the associated spectral function evolves from one peak in the Fermi-liquid regime to two peaks in the fluctuation regime. In addition, the antisymmetric structure of the imaginary part of the susceptibility used by Kampf and Schrieffer is reminiscent of the behavior of the imaginary part of our pair-fluctuation propagator in the weak-coupling regime only.

Further detailed ARPES (and, possibly, inverse photoemission) experiments are awaited to ultimately distinguish the microscopic origin of the pseudogap in underdoped cuprates and to unambiguously identify the characteristic features of the spectral function obtained by our analysis in different doping and coupling regimes.

#### ACKNOWLEDGMENTS

The authors are indebted to A. A. Varlamov for discussions. A.P. gratefully acknowledges financial support from the Italian INFM under Contract No. PAIS Crossover No. 269.

- 
- <sup>1</sup>For a recent review, see T. Timusk and B. Statt, *Rep. Prog. Phys.* **62**, 61 (1999).
- <sup>2</sup>H. Ding, T. Yokoya, J. C. Campuzano, T. Takahashi, M. Randeria, M. R. Norman, T. Mochiku, K. Hadowaki, and J. Giapintzakis, *Nature (London)* **382**, 51 (1996).
- <sup>3</sup>M. R. Norman, H. Ding, M. Randeria, J. C. Campuzano, T. Yokoya, T. Takeuchi, T. Takahashi, T. Mochiku, K. Kadowaki, P. Guptasarma, and D. G. Hinks, *Nature (London)* **392**, 157 (1998).
- <sup>4</sup>J. C. Campuzano, H. Ding, M. R. Norman, H. M. Fretwell, M. Randeria, A. Kaminski, J. Mesot, T. Takeuchi, T. Sato, T. Yokoya, T. Takahashi, T. Mochiku, K. Kadowaki, P. Guptasarma, D. G. Hinks, Z. Konstantinovic, Z. Z. Li, and H. Raffy, *Phys. Rev. Lett.* **83**, 3709 (1999).
- <sup>5</sup>Ch. Renner, B. Revaz, J.-Y. Genoud, K. Kadowaki, and Ø. Fischer, *Phys. Rev. Lett.* **80**, 149 (1998).
- <sup>6</sup>N. Miyakawa, P. Guptasarma, J. F. Zasadzinski, D. G. Hinks, and K. E. Gray, *Phys. Rev. Lett.* **80**, 157 (1998); N. Miyakawa, J. F. Zasadzinski, L. Ozyuzer, P. Guptasarma, D. G. Hinks, C. Kendziora, and K. E. Gray, *ibid.* **83**, 1018 (1999).
- <sup>7</sup>F. Pistolesi and G. C. Strinati, *Phys. Rev. B* **49**, 6356 (1994).
- <sup>8</sup>F. Pistolesi and G. C. Strinati, *Phys. Rev. B* **53**, 15 168 (1996).
- <sup>9</sup>N. Andrenacci, A. Perali, P. Pieri, and G. C. Strinati, *Phys. Rev. B* **60**, 12 410 (1999).
- <sup>10</sup>M. Randeria, J.-M. Duan, and L.-Y. Shieh, *Phys. Rev. Lett.* **62**, 981 (1989).
- <sup>11</sup>M. Randeria in *Bose-Einstein Condensation*, edited by A. Griffin *et al.* (Cambridge University Press, Cambridge, 1995).
- <sup>12</sup>M. Randeria, in *Proceedings of the International School of Physics "Enrico Fermi,"* edited by G. Iadonisi *et al.* (IOS, Amsterdam, 1998).
- <sup>13</sup>J. O. Sofo and C. A. Balseiro, *Phys. Rev. B* **45**, 8197 (1992).
- <sup>14</sup>M. Capezali and H. Beck, *Physica B* **259-261**, 501 (1999).
- <sup>15</sup>B. Jankó, J. Maly, and K. Levin, *Phys. Rev. B* **56**, R11 407 (1997).
- <sup>16</sup>Q. Chen, I. Kosztin, B. Jankó, and K. Levin, *Phys. Rev. Lett.* **81**, 4708 (1998).
- <sup>17</sup>J. Maly, B. Jankó, and K. Levin, *Physica C* **321**, 113 (1999).
- <sup>18</sup>T. Hotta, M. Mayr, and E. Dagotto, *Phys. Rev. B* **60**, 13 085 (1999).
- <sup>19</sup>Y. Yanase and K. Yamada, *J. Phys. Soc. Jpn.* **68**, 2999 (1999).
- <sup>20</sup>A. Ino, C. Kim, M. Nakamura, T. Yoshida, T. Mizokawa, A. Fujimori, Z.-X. Shen, T. Kakeshita, H. Eisaki, and S. Uchida, cond-mat/0005370 (unpublished).
- <sup>21</sup>T. Valla, A. V. Fedorov, P. D. Johnson, Q. Li, G. D. Gu, and N. Koshizuka, *Phys. Rev. Lett.* **85**, 828 (2000).
- <sup>22</sup>J. C. Campuzano, H. Ding, M. R. Norman, M. Randeria, A. F. Bellman, T. Yokoya, T. Takahashi, H. Katayama-Yoshida, T. Mochiku, and K. Kadowaki, *Phys. Rev. B* **53**, R14 737 (1996).
- <sup>23</sup>A. Perali, C. Castellani, C. Di Castro, M. Grilli, E. Piegari, and A. A. Varlamov, *Phys. Rev. B* **62**, R9295 (2000).
- <sup>24</sup>V. Emery and S. A. Kivelson, *Nature (London)* **374**, 434 (1995).
- <sup>25</sup>V. M. Loktev, R. M. Quick, and S. G. Sharapov, *Phys. Rep.* **349**, 1 (2001).
- <sup>26</sup>M. Franz and A. J. Millis, *Phys. Rev. B* **58**, 14 572 (1998).
- <sup>27</sup>H. J. Kwon and A. T. Dorsey, *Phys. Rev. B* **59**, 6438 (1999).
- <sup>28</sup>R. Micnas, M. H. Pedersen, S. Schafroth, and T. Schneider, J. J. Rodríguez-Núñez, and H. Beck, *Phys. Rev. B* **52**, 16 223 (1995).
- <sup>29</sup>J. M. Singer, M. H. Pedersen, T. Schneider, H. Beck, and H.-G. Matuttis, *Phys. Rev. B* **54**, 1286 (1996).
- <sup>30</sup>Y.-M. Vilk, S. Allen, H. Touchette, S. Moukouri, L. Chen, and A.-M. S. Tremblay, *J. Phys. Chem. Solids* **59**, 1873 (1998).
- <sup>31</sup>B. Kyung, S. Allen, and A.-M. S. Tremblay, *Phys. Rev. B* **64**, 075116 (2001).
- <sup>32</sup>3D fluctuations are weaker than 2D ones as  $T \rightarrow T_c$ . However, if critical properties are not of interest, the strength of 3D fluctua-

- tions can be increased by increasing coupling.
- <sup>33</sup>P. Pieri and G. C. Strinati, Phys. Rev. B **61**, 15 370 (2000).
- <sup>34</sup>For a recent review on superconducting fluctuations, see A. A. Varlamov, G. Balestrino, E. Milani, and D. V. Livanov, Adv. Phys. **48**, 1 (1999).
- <sup>35</sup>P. Nozieres and S. Schmitt-Rink, J. Low Temp. Phys. **59**, 195 (1985).
- <sup>36</sup>The imaginary part of  $\Gamma^{(0)}(\mathbf{q}, \omega)$  in Eq. (5) is meant to be obtained from the expression (2) with the replacement  $i\Omega_\nu \rightarrow \omega + i\eta$  (where  $\eta$  is a positive infinitesimal). In this way, one can show that it is possible to write the spectral representation  $-\pi\Gamma^{(0)}(\mathbf{q}, i\Omega_\nu) = \int_{-\infty}^{\infty} d\omega \text{Im} \Gamma^{(0)}(\mathbf{q}, \omega) (i\Omega_\nu - \omega)^{-1}$ , even though  $\Gamma^{(0)}(\mathbf{q}, i\Omega_\nu)$  cannot be considered to be a Green's (or a correlation) function in the usual sense. (A related discussion on the analytic properties of  $\Gamma^{(0)}$  has been presented in Ref. 37.)
- <sup>37</sup>D. Rohe and W. Metzner, Phys. Rev. B **63**, 224 509 (2001).
- <sup>38</sup>S. Moukouri, S. Allen, F. Lemay, B. Kyung, D. Poulin, Y. M. Vilks, and A.-M. S. Tremblay, Phys. Rev. B **61**, 7887 (2000).
- <sup>39</sup>Analogous results for the critical chemical potential  $\mu_c(T)$  as a function of temperature have been obtained by S. Schmitt-Rink, C. M. Varma, and A. E. Ruckenstein [Phys. Rev. Lett. **63**, 445 (1989)] for a *two*-dimensional Fermi gas with an attractive *s*-wave interaction.
- <sup>40</sup>M. Letz and R. J. Gooding, J. Phys.: Condens. Matter **10**, 6931 (1998).
- <sup>41</sup>R. Haussmann, Phys. Rev. B **49**, 12 975 (1994).
- <sup>42</sup>R. Haussmann, Z. Phys. B: Condens. Matter **91**, 291 (1993).
- <sup>43</sup>In terms of the phenomenological parameter  $k_F \xi_{\text{pair}}$ , the value  $(k_F a_F)^{-1} \approx 2$  corresponds to  $k_F \xi_{\text{pair}} \approx 0.4$ , which is close to the value  $k_F \xi_{\text{pair}} = 1/\pi$  separating the crossover region from the BE regime at  $T=0$ , as discussed in Ref. 7.
- <sup>44</sup>M. Marini, F. Pistolesi, and G. C. Strinati, Eur. Phys. J. B **1**, 151 (1998).
- <sup>45</sup>It can be readily verified that the analytic continuation of the self-energy (1) vanishes when  $|\omega| \rightarrow \infty$ . For this reason, there is no additional constant shift to be added to  $\Sigma_0$ , when the real part of  $\Sigma(\mathbf{k}, \omega)$  is calculated as the Kramers-Kronig transform of the imaginary part (5).
- <sup>46</sup>A. Schmid, Z. Phys. **231**, 324 (1970).
- <sup>47</sup>I. Vobornik, H. Berger, M. Grioni, G. Margaritondo, L. Forró, and F. Rullier-Albenque, Phys. Rev. B **61**, 11 248 (2000).
- <sup>48</sup>N. Andrenacci, P. Pieri, and G. C. Strinati, Eur. Phys. J. B **13**, 637 (2000).
- <sup>49</sup>M. R. Norman, H. Ding, H. Fretwell, M. Randeria, and J. C. Campuzano, Phys. Rev. B **60**, 7585 (1999).
- <sup>50</sup>M. R. Norman, M. Randeria, H. Ding, and J. C. Campuzano, Phys. Rev. B **57**, R11 093 (1998).
- <sup>51</sup>B. R. Patton, Phys. Rev. Lett. **27**, 1273 (1971).
- <sup>52</sup>S. Caprara, M. Sulpizi, A. Bianconi, C. Di Castro, and M. Grilli, Phys. Rev. B **59**, 14 980 (1999).
- <sup>53</sup>Note that the existence of preformed pairs above  $T_c$  is also a possible outcome of the stripe-based scenario. If underdoped cuprates are near a stripe-instability line at temperature  $T_{\text{CDW}}$ , in fact, the dynamical charge fluctuations arising above  $T_{\text{CDW}}$  can mediate and sustain strong pairing up to a higher temperature  $T^* > T_{\text{CDW}}$  [C. Castellani, C. Di Castro, and M. Grilli, Z. Phys. **130**, 107 (1997)].
- <sup>54</sup>D. Pines, Z. Phys. B: Condens. Matter **103**, 129 (1997), and references quoted therein.
- <sup>55</sup>A. Kampf and J. R. Schrieffer, Phys. Rev. B **41**, 6399 (1990).
- <sup>56</sup>J. R. Schrieffer and A. P. Kampf, J. Phys. Chem. Solids **56**, 1673 (1995).